2016

Determination of stiffness reduction factor for U-shaped reinforced concrete shear walls under bi-axial loading

Sai Krishna Yemmaleni
Iowa State University

Determination of stiffness reduction factor for U-shaped reinforced concrete shear walls under bi-axial loading

by

Sai Krishna Yemmaleni

A thesis submitted to the graduate faculty

in partial fulfillment of the requirements for the degree of

MASTER OF SCIENCE

Major: Civil Engineering (Structural Engineering)

Program of Study Committee:

In Ho Cho, Major Professor

Sri Sritharan

Jeramy Ashlock

Iowa State University

Ames, Iowa

2016

TABLE OF CONTENTS

LIST OF FIGURES

Page

LIST OF TABLES

ACKNOWLEDGMENTS

I would like to thank my Major Professor, Dr. In Ho Cho, and my committee members, Dr. Sri Sritharan, and Dr. Jeramy Ashlock for their guidance and support throughout the course of this research.

In addition, I would also like to thank my friends, colleagues, the department faculty and staff for making my time at Iowa State University a wonderful experience. I want to also offer my appreciation to those who were willing to participate in my surveys and observations, without whom, this thesis would not have been possible.

ABSTRACT

Reinforced Concrete (RC) shear wall, is an effective primary earthquake resisting system due to strong stiffness and large shear-force resisting capacity. For a complex asymmetric wall, severe damage on a portion of the wall may directly affect the stiffness in other directions. Such a secondary damage mechanism is hard to capture. Hence, this study was devoted to determining a stiffness reduction index that can monitor current damage state of the wall system as a whole, and apply the unified damage index to decrease stiffness and strength on other directions. This study proposes an analytical framework at microscopic length scale that is based on a unit cell which consists of nonlinear steel spring, compression only gap, and concrete compression spring. For validation and applications, three U-shaped wall specimens available in literature (designed according to EC8) were modeled and simulated under cyclic lateral loading. These walls have the same dimensions and reinforcement except for the different loading directions. The present study concludes that the proposed unit cell model appears to be successful for predicting the stiffness reductions resulting from localized damages in different loading directions. The proposed unit cell-based framework seems to be a good starting point to consider secondary stiffness reductions for other complex non-rectangle walls such as L-, H- and T-shaped walls. This method may facilitate the fast determination of remaining stiffness of complex RC walls by using quick post-disaster observations.

CHAPTER 1
INTRODUCTION

1.1 **Reinforced Concrete Shear Walls**

Reinforced concrete (RC) shear walls are often used as the primary lateral load-resisting system in structures because of their significant in-plane stiffness, which enables them to resist lateral loads effectively while limiting lateral deformations. In many cases, shear walls with foundations of adequate strength to prevent overturning, may not practically be designed to respond elastically to design level ground shaking. In regions with a high seismic hazard, rectangular cross section walls are seldom used, if as an exception, walls with rectangular cross section are used they often need large reinforcement ratios. The importance of the ductility properties of the longitudinal reinforcement on the displacement capacity of the walls was for a long time undervalued and reinforcing steel was merely rated for its strength rather than its deformation capacity. As a consequence, a portion of the existing RC wall buildings was constructed with reinforcing steel possessing inferior ductility properties. Over the last decades, the seismic behavior of RC shear walls with rectangular cross section with varying parameters (ductility) has been the subject of extended research and several test series [e.g. *Dazio et. al., 2009* [1]; *Aaleti et. al., 2013* [14]; *Salonikos et. al., 1996* [15] on such walls were conducted. From the results of these experimental data, the key parameters controlling the behavior of rectangular walls could be inferred. The results also proved that highly ductile walls need to be constructed in regions of high seismicity to attain higher capacity [1]. Because of its simple geometry rectangular walls behavior under biaxial and uniaxial loading is quite similar.

Walls of complex geometry like (U-, T-, L-, or H- shaped sections) are also quite common in earthquake-resistant concrete buildings. Such non-rectangle walls are intended to provide stiffness and resistance in both horizontal directions, and their bi-directional behavior under seismic actions is more complex than that of rectangular walls. The behavior of non-rectangular walls under uniaxial and biaxial loading is not adequately known, as the quantity of observational and numerical studies are truly less. These non-rectangular walls were designed for medium ductility according to an older version. However, experimental study proves that high ductile reinforced concrete non-rectangular walls provide higher capacity [2].

For shear walls, the effective action is shear and the ACI 318 method for shear walls is based on empirical expressions derived originally for beams by using test results usually exhibiting a broad scatter. The ACI provisions for the design of reinforced concrete squat walls are in disagreement with the observed structural behavior. While the codes suggest the shear resistance of the wall is due to the tensile strength of concrete, *Lefas et. al.*, 1990 [31] has shown that the shear resistance of the wall is mainly due to the concrete compressive strength in the compression zone. He also proved that the web reinforcement does not have a significant effect on the shear force capacity.

Hence, computational investigation of the dynamic behavior of RC shear walls is crucial for design purpose. The seismic performance assessment and loss computations of shear walls are done using fragility functions. Fragility functions relate the probability of exceeding one or more damage thresholds (described using damage states and repair measures) to a demand parameter such as story drift or component plastic deformation[34]. Damage states are characterized typically using descriptors such as crack width, the extent of concrete crushing, sliding shear displacement and reinforcement yielding and buckling. The fragility curves usually presented as a function of increasing drift, which is the best single story-level demand parameter for most structural elements such as walls. Drift is the demand parameter most reported in the literature. Four damage states and corresponding method of repairs have been defined based on the shear wall response to quasi-static loading [3]. Many analytical models have been proposed for the nonlinear dynamic analysis of structures. A review of existing analytical studies relevant to the nonlinear seismic response of RC shear walls is presented in the following. These models have proven to provide valuable understanding on the dynamic behavior of RC shear walls. Because several parameters in the model are assumed through personal testing, reliability might be limited[35]. Respecting a chronological order, lumped plasticity models are presented first, and distributed nonlinearity models follow[4].

1.2 **Lumped Models:**

Under seismic excitation, the inelastic behavior of reinforced concrete frames often concentrates at the ends of beams and columns. Thus, a fresh approach to modeling this behavior was to use plastic hinges in the form of nonlinear springs located at the member ends. Several lumped plasticity constitutive models have been proposed to date[17,18,19,20,21,22]. Such models

include cyclic stiffness degradation in flexure and shear[4], pinching under reversal and fixed end rotations at the beam-column joint interface due to bar pull-out. Axial-flexural coupling is neglected. The advantage of lumped model is its simplicity that reduces storage requirements and computational costs and improves the numerical stability of the computations. Most lumped models, however, oversimplify certain important aspects of the hysteretic behavior of reinforced concrete members and are therefore limited in applicability. Parametric and theoretical studies of beams under monotonic loading demonstrate a strong dependence between model parameters and the imposed loading pattern and level of inelastic deformation. Neither of the factors is likely to remain constant during the dynamic response. The problem is further strengthened by the fluctuation of the axial force in the columns. Because of this history of dependence, damage predictions at the global, but especially at the local level, may be grossly inaccurate.

1.2.1 **Fiber Hinge Model**: To overcome some of the limitations in lumped models *Lai et. al* [23]. proposed fiber hinge model that consists of a linear elastic element extending over the entire length of the reinforced concrete member and has one inelastic spring at each end. Each inelastic element is made up of one inelastic spring at each section corner that represents the longitudinal reinforcing steel and central concrete spring that is effective in compression only. The five spring discretization of the end sections is capable of simulating the axial force- biaxial bending moment interaction in reinforced concrete members in a more rational way that is possible by classical plasticity theory.

1.3 **Distributed Nonlinear Model:**

A more accurate description of the inelastic behavior of reinforced concrete members is possible with distributed nonlinearity models [21, 24, 25, 26, 27, 22, 28]. In contrast to the lumped model, material nonlinearity can take place at any element section, and the element behavior is derived by weighted integration of the section response. The constitutive behavior of the cross section is either formulated by classical plasticity theory regarding stress and strain resultants or is explicitly derived by discretization of the cross section of fibers. A common assumption is that plane section remains plane, such that the strains are linearly distributed over the cross section. Of the different models proposed by other authors [4] the most promising model is the fiber section model.

1.3.1 **Fiber Section Model:**

The most prominent model for the nonlinear analysis of reinforced concrete members presently the flexibility- based fiber section model. In this model, the RC structural member is divided into several longitudinal sections, and each section is comprised of several fibers as shown in Figure1. This model has been widely accepted to RC members whose failure is predominately controlled by flexure behavior. Each fiber has its uniaxial constitutive law and different fibers in the same section follow the assumption that 'plane section remains plane.'

It is important to note that brittle shear failure is considered in the proposed fiber- beam mode. When the internal shear force exceeds the prescribed shear strength of the fiber- beam element, the strength and the stiffness of the element abruptly falls to zero. The stress- strain model proposed by *Legeron et.al*, [29] is used in this study to model the backbone curve of concrete. The stress-strain model proposed by *Esmaeily et. al.* and *Xiao et. al.* [30] is adopted to model the backbone curve of steel. The model proposed by *Legeron et.al.* is taken to model the unloading and reloading paths. For complete formulation, refer to [4]**.**

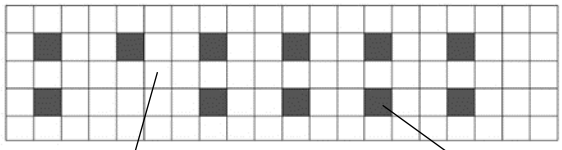

Figure 1: Rectangular Section divided into fibers.

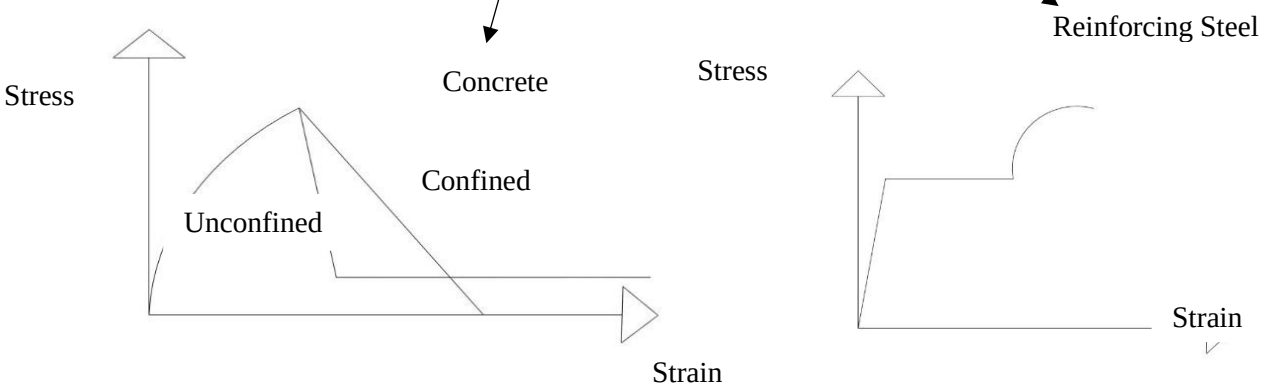

Figure 1.1: Steel and Concrete stress- strain plot associated to a fiber

1.4 **Multilayered Shell Element**

The Multi-layered shell model is based on the principles of composite material mechanics and is capable of simulating coupled in-plane/out-of-plane bending and in-plane direct shear and coupled bending-shear behavior of RC walls. [5] The multi-layered shell element is made up of a number of layers with different thickness and material properties (Figure 2). The rebar is smeared into one or more layers, and these rebar's layer can either be isotropic or orthotropic depending on the reinforcement ratio in the longitudinal and transverse directions

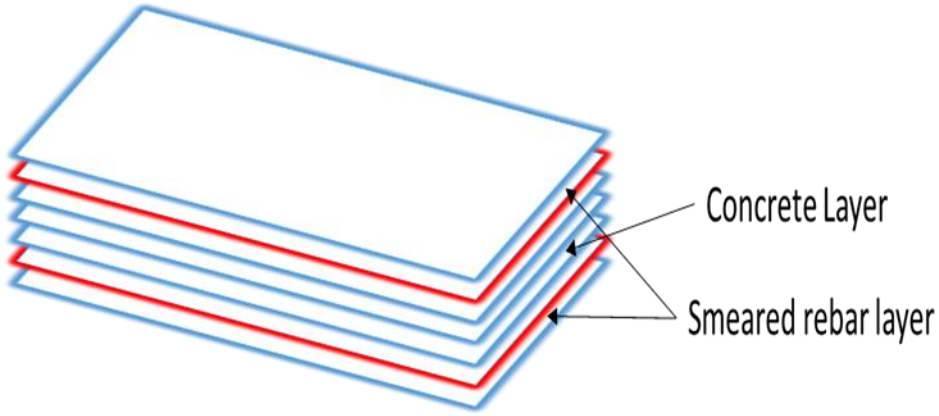

Figure 2: FE Section of the wall modeled by Multilayered Shell Element

The multi-layer shell formulation is based on the "ShellMITC4" element [6], which is a four-node shell element builds on the theory of is a mixed interpolation of tensorial components. For complete formulation refer to [5, 6].

Drawback: In the multi-layered shell element as all the rebar properties are smeared into one layer; it cannot capture localized damages like bar buckling which are critical in understanding the collapse mechanism of the wall. These models are found to mesh sensitive[16] highly. Hence, it is required to fix the mesh size before moving ahead with the analysis.

1.5 **Virtual Earthquake Engineering Tool (VEEL):**

Based on the limitations described above, *Cho et. al.*, embarked upon the development of a structure-independent parallel platform called Virtual Earthquake Engineering Tool (VEEL). This platform is imbued with a number of microphysical mechanisms. To fully retain the physical nature of real cracks, Cho adopted fixed type multi-directional smeared crack model,

smart bar model to capture progressive bar buckling, confinement model to take into consideration the confinement effect. For in-depth information and formulation, please refer to Cho's papers [5,6,7,8, 9, 10, 12]**.** The simulation of this platform is done using parallel computers and a novel algorithm developed by Cho termed as multilayered grouping parallel algorithm [5]. The walls are modeled using an automated meshing program developed by *Cho* [7]. For this study, VEEL platform is preferred for the simulation study as it is very easy to model complex U-shaped walls, assign concrete and steel properties with no artificial definition of core and cover concrete.

1.6 **Objective:**

The behavior of U-shaped walls subjected to uniaxial and biaxial cyclic loading is different compared to a rectangular wall. Because of it asymmetrical wall geometry, damage caused by one directional load may causes a significant stiffness reduction in other direction. An intense research was devoted to determining a stiffness reduction index that can monitor current damage state of the wall system as a whole, and apply the unified damage index to decrease stiffness and strength on other direction.

This thesis proposes a new and efficient analytical framework that can swiftly predict the remaining stiffness in all directions after a localized damage took place by one directional loading at a portion of a U-shaped wall system. To meet this goal, this study proposes a microscopic unit cell that consists of nonlinear steel spring, compression-only gap, and concrete compression spring. For validation and application, this study presents in-depth modeling and analysis of U-shaped RC walls. Then validation is done by comparing the simulated results of X, Y and biaxial loading force displacement graphs with the experimental data. The level of damage with increasing drift ratio on YZ and XZ plane of Wall1 and Wall2 is determined by plotting the contor plots. Then specific formulation on the derivation of unified damage index for both 1D and 2D loading based on spring molecule model is presented. A parametric study of cell size and concrete stiffness reduction factor (d) is conducted, and an optimal setting was determined which matches with the experimental results. Finally, validating the numerical result with the experimental result is done, for the secondary stiffness.

CHAPTER 2

FINITE ELEMENT MODELLING AND SIMULATION RESULTS

2.1 **Test Specimen**

A total of three U-shaped wall specimens were modeled and simulated under cyclic lateral loading. All the three walls have the same dimensions and reinforcement, but the direction of loading is different in each case. The test specimens have been designed according to EC8 code.

Geometrical details of the U-Shaped Wall [13] are given in Table 1.

Table 1: Geometric details of U- Shaped Wall

Description	Dimensions(mm)
Flanges Length	1250
Flange Thickness	250
Web Length	1500
Web Thickness	250
Height	3600
Concrete cover	25

The configuration and arrangement of the reinforcement are shown in Figure 3.

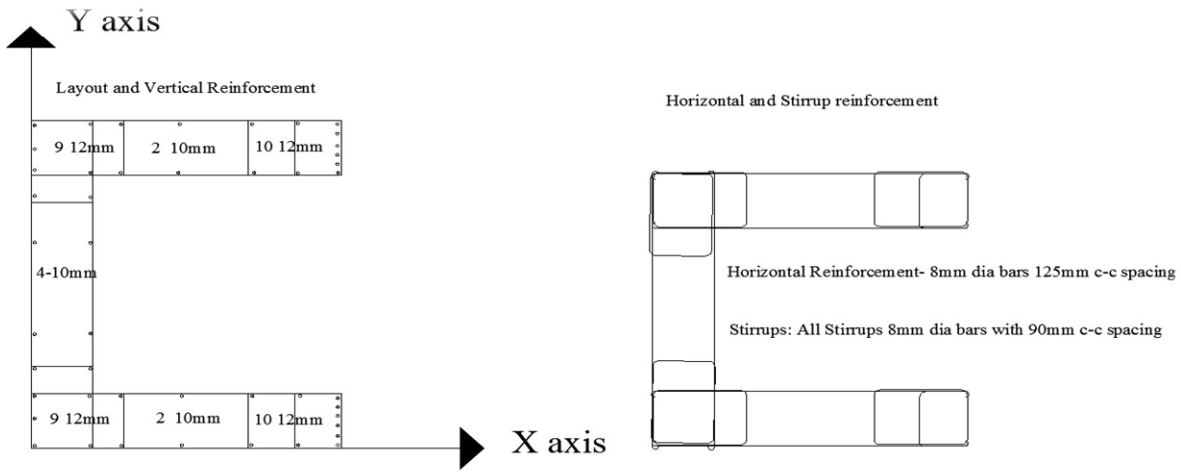

Figure 3: Section details of wall test specimen

Reinforcement details: 10mm and 12mm diameter bars with an overall steel ratio (ρ) = 0.0056 over the section were used as vertical rebar in the boundary and web portion of the walls. Horizontal steel reinforcement: two curtains of 8mm diameter bars at 125mm spacing center to center in the flanges and at 75mm spacing center to center in the web. Confinement reinforcement: 8mm diameter bars at 90mm center to center spacing were used as horizontal reinforcement. [13]

2.2 **Modelling and Meshing**

The finite element model of the U-shaped wall is done using General Auto Meshing Preprocessor Tool, developed by Cho [7]. Figures 2a & 2b, convey the geometry and actual reinforcement layout of the U-shaped wall under consideration. The concrete part is modeled by hexahedral solid elements while the entire reinforcing bar system (i.e. vertical, horizontal and confinement reinforcement) is explicitly modeled by space trusses. Importantly the pre-processing tool includes the data input task (like the material and hysteresis properties, loading history, nodal force, and nodal reference force) with the aid of an automated meshing program developed by Cho **[**8]

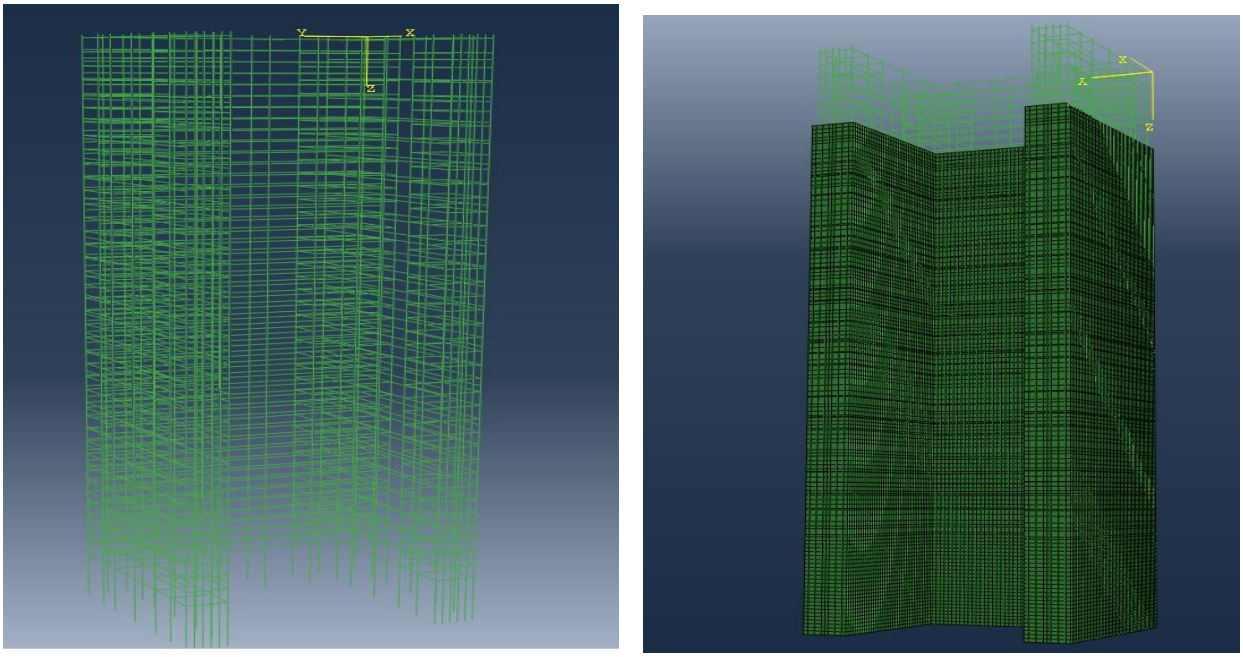

Figure 4: Mesh of reinforcement bars of the U- Shaped Wall

Each wall (i.e. Wall1, Wall2, and Wall3) was modeled with 218214 solid elements and 193200 truss elements.

2.3 **Material and Hysteresis Properties**

After generating the input file, we need to input the material and hysteresis properties for concrete and all the steel bars of the U-shaped wall referring to [13]

Concrete Properties: Based on modified thorenfeldt concrete model with non-local-information-based confinement model. This choice has been made because the model is believed to be one of the most balanced models with sufficient accuracy and efficiency for concrete, covering a broad range of strengths [12]. The properties inputted for concrete are summarized in Table 2.

Table 2: Concrete properties for the test specimen from [13]

Modulus of Elasticity (E_c)	28.0GPa
Poison's Ratio	0.2
Density	2286.0 kg/m^3
Thermal Coefficient	0.23
Compressive Strength (*fc*)	23.73 MPa
Compressive Strain (ε_c)	-0.002

Rebar Properties: All the vertical reinforcement (i.e. Φ12mm and Φ10mm bars) were based Menegotto-Pinto steel model with compressive buckling Cho [8]. All the horizontal reinforcement and stirrups (i.e. Φ8mm bars) were based on bilinear steel model. The properties entered for the rebar are summarized in Table 3.

Table 3: Steel rebar properties referring to [13]

Description	Φ12mm	Φ10mm	Φ8mm
Area	113.097×10^{-6} m^2	78.5398×10^{-6} m^2	50.2655×10^{-6} m^2
Yield Stress (σy)	516 MPa	525 MPa	557 MPa
Yield Strain (εy)	0.002	0.002	0.002
Reduction factor(b)	0.00156	0.00146	0.00123
Ultimate stress (σu)	615 MPa	617 MPa	642 MPa

2.4 **Loading Conditions**

The three specimens (i.e. Wall1, Wall2, and Wall3) having the same geometry, reinforcement, and material properties were subjected to three cyclic tests: a uniaxial cyclic test in the Y direction, a uniaxial cyclic test in the X direction and a biaxial cyclic test in the XY direction. The lateral loading point for all the three walls is at 3.9m from the ground level. A vertical axial load of 2 MN was applied for all the three walls. Hence, the axial force ratio is equal to 0.0963.

The loading history for each case is shown in [Figures 5,6,7,8]

Wall1 – Loaded in the Y direction (as per VEEL coordinate system)

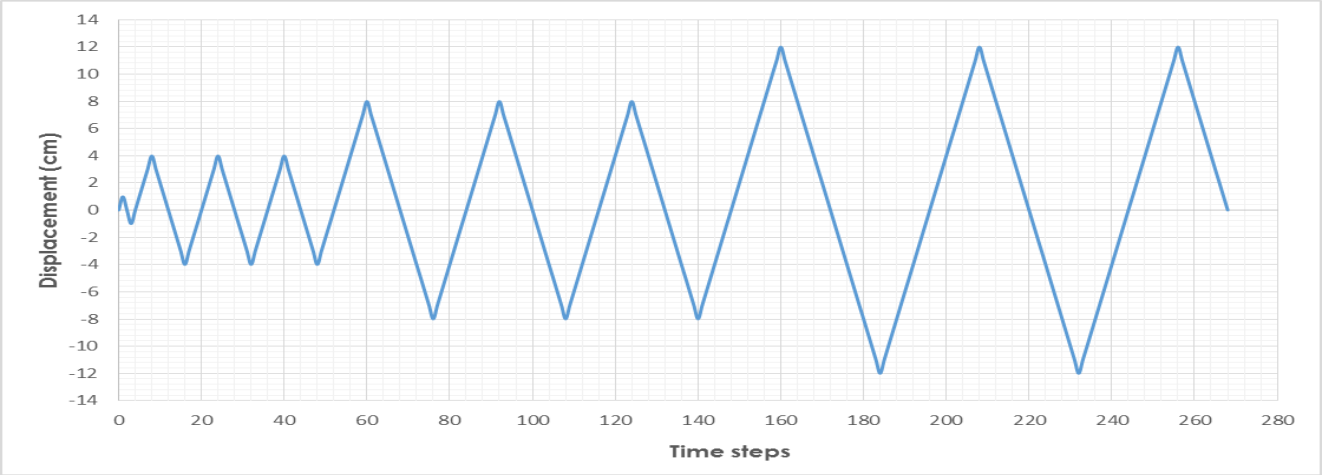

Figure 5: Horizontal displacement vs. time history- Y direction

Wall2- Loaded in the X direction (as per VEEL coordinate system)

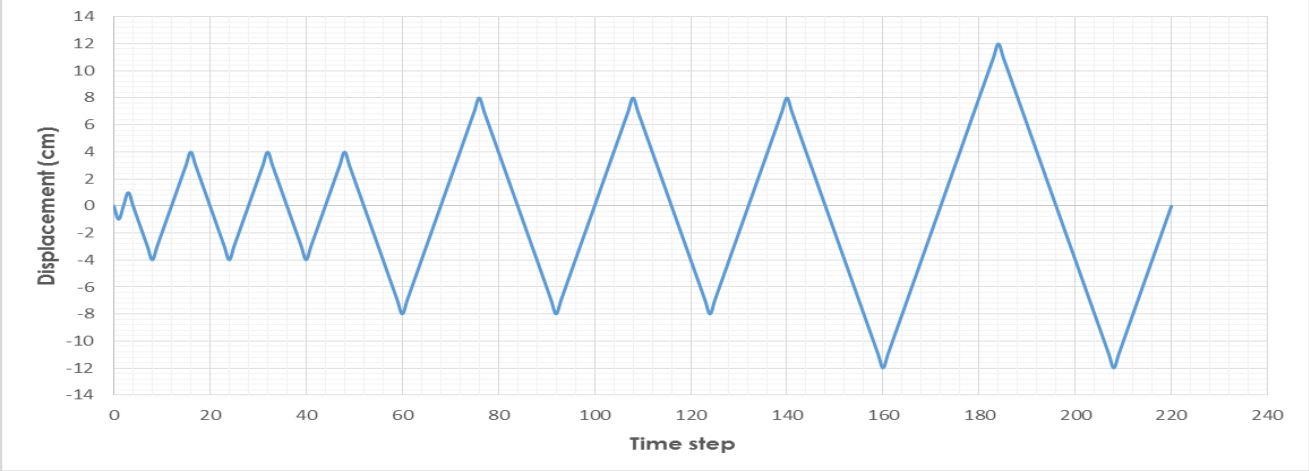

Figure 6: Horizontal displacement vs. time history – X direction.

Wall3- biaxial cyclic loading in both XY Direction

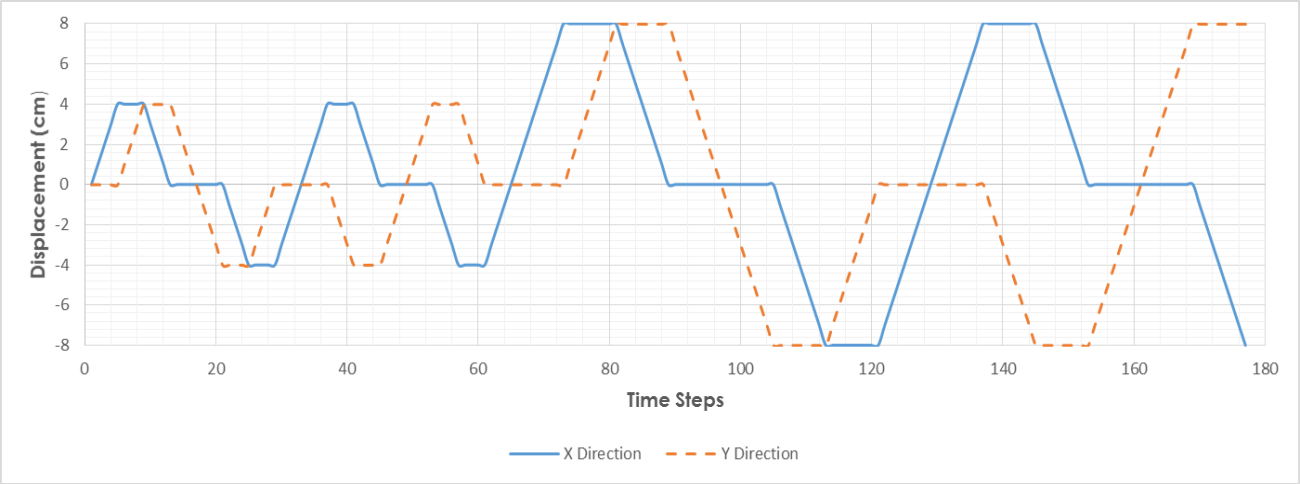

Figure 7: Average horizontal displacements time histories: XY biaxial test

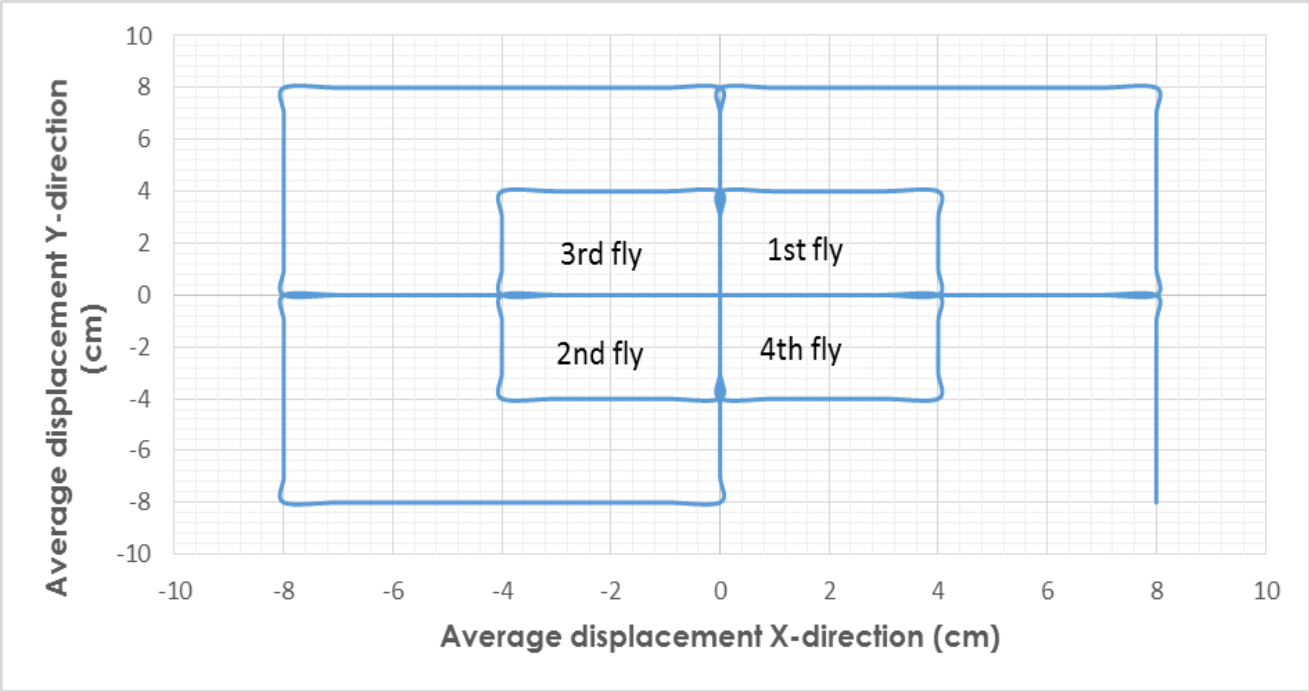

Figure 8: Y top displacement vs X top displacement: XY biaxial test.

2.5 **Validating simulation result with experimental result**

Simulation of the three walls was performed on High-Performance Computer (HPC) condo cluster provided by Iowa State Research IT group. The HPC Condo cluster is composed of 144 computer nodes, in addition to the head node, data transfer node, a large memory node, and a large memory node. Each of the nodes is connected via Intel QDR InfiniBand (40Mbps) switch, and run Red Hat Enterprise Linux 6 [33]. The simulation was on six nodes, and each node consists of 16 processors, therefore making total CPU's equals 96. The total number of displacement time steps to obtain the nonlinear response of the walls was set to 268, 440 and 177 for Wall1, Wall2, and Wall3 respectively.

After complete simulation, using a postprocessor developed by Cho [8]. The force vs. displacement response was obtained for each of the three cases and compared with the experimental results [13]**.**

Case 1: Wall1 - (Y-Direction Loading)

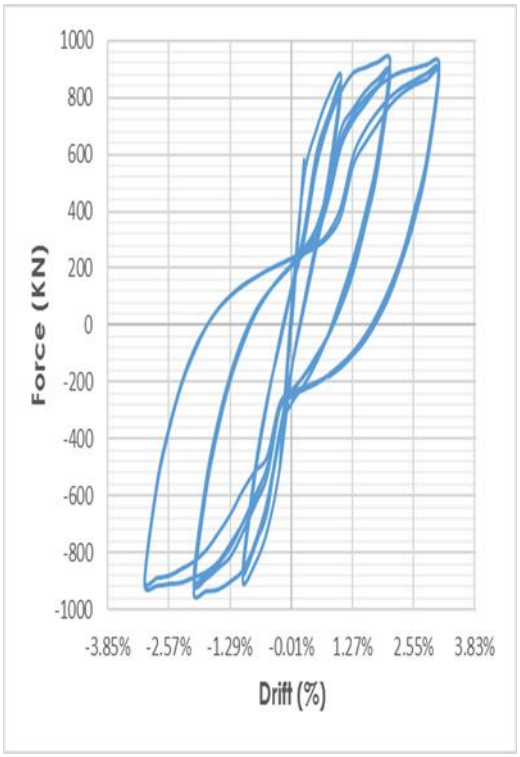

Figure: 9 (a): simulation result- VEEL

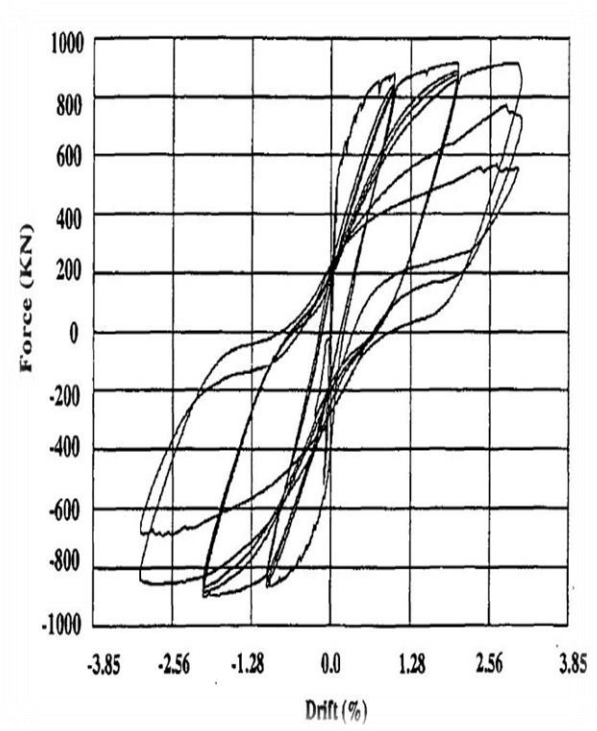

Figure 9(b): Experimental Result

Source: N. ILE [13]

From Figures 9(a) and 9(b), we see that the overall shape and range of the simulated force-displacement (FD) hysteresis loop coincides well with the experimental result when the wall is subjected in Y- direction loading. Experimentally the first cracking was observed at about 1cm displacement during the first loading cycle. At 8cm displacement, some buckling occurred.The U-shaped wall failure, occurred when three vertical bars on the flange side broke while straightening back up after buckling in compression. The resulting displacement ductility factor was found to be of approximately 6. One of the differences in the experimental and simulation results is that there is no stiffness degradation in VEEL result compared to the experimental result. One plausible cause for this differences is that the VEEL assumes a perfect bond between concrete and steel which may not be the case in the experimental setup. Other than this issue, we can conclude that VEEL is a useful tool for predicting the cyclic behavior of non-rectangular shear walls.

Case 2: Wall2 -(X-Direction Loading)

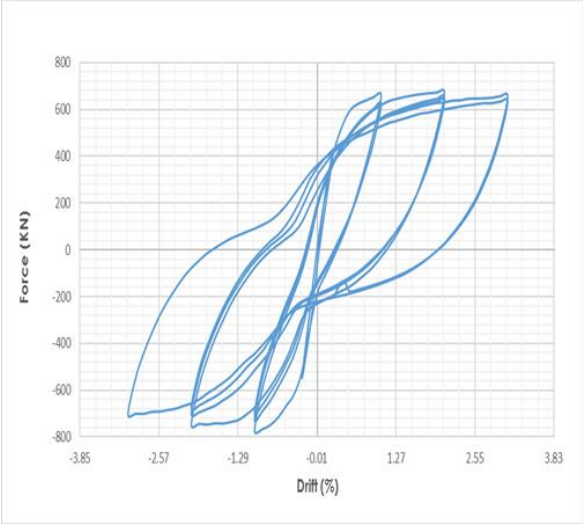

Figure 10 (a): Simulation Result

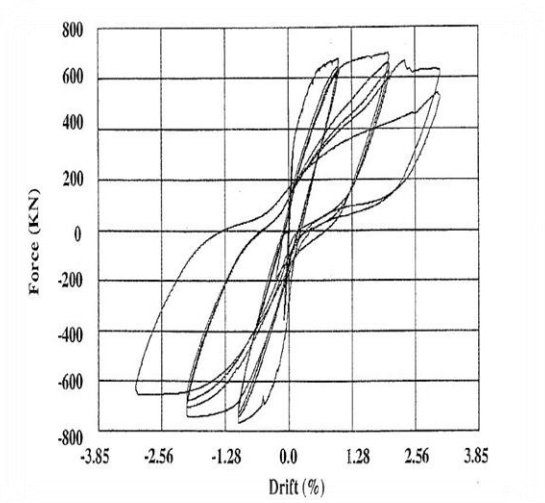

Figure 10(b): Experimental Result

Source: N. ILE [13]

From Figures 10(a) and 10(b), we see that the overall shape of the simulated force-displacement graph coincides well with the experimental result when the wall is subjected to X- direction loading. The ranges both force as well as displacement match reasonable well. Experimentally, the first inclined cracking at the base of the flanges was observed at about 2cm displacement during the first loading cycle. The specimen failed in the X positive direction of loading, by the

bars buckling on the corner. of the U-shaped wall web. The resulting displacement ductility factor is found to be approximately 6cm. The only difference that can be observed is the stiffness degradation in the experimental result which couldn't be predicted in VEEL because of the assumption of the perfect bond between steel and concrete. Hence, further development is required in the VEEL platform, considering the bond slip so that the simulation result exactly matches with the experimental result.

3. Wall3- (XY Loading)

along Y Direction

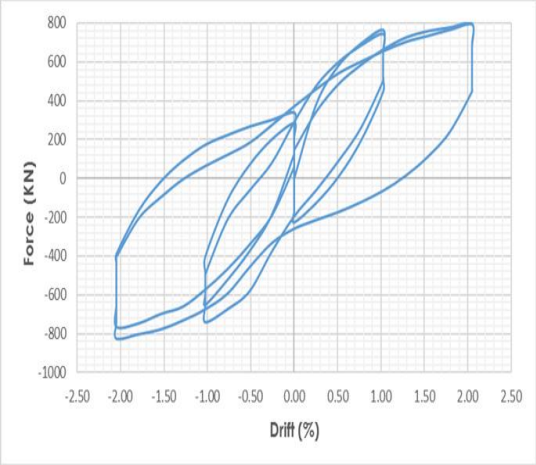

Fig: 11(a): Simulation Result

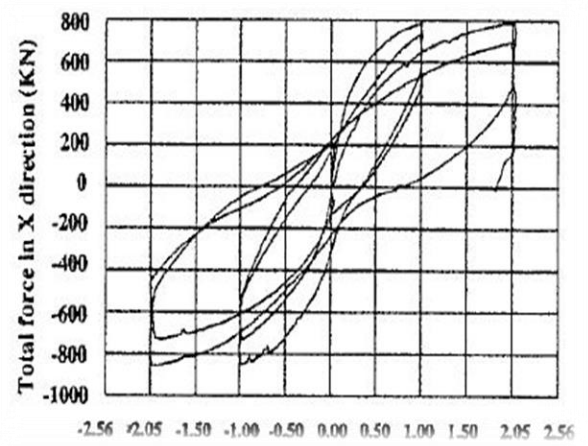

Fig 11(b): Experimental Result

Source: N.ILE [13]

along X Direction

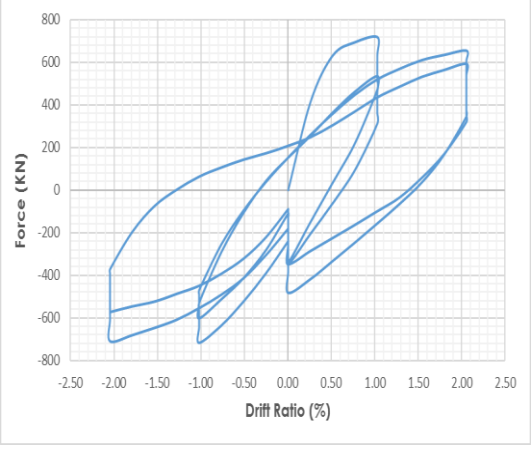

Fig 12(a): Simulation Result

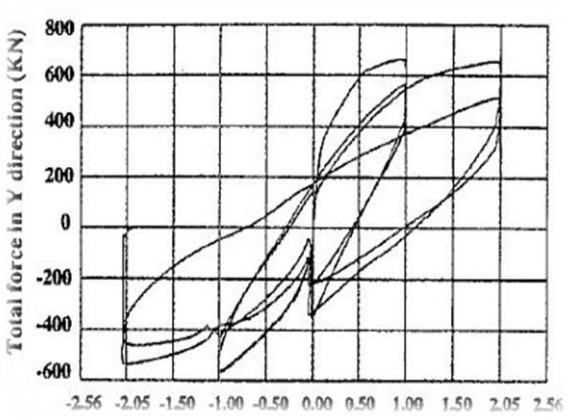

Fig 12(b): Experimental Result.

Source: N.ILE [13]

Wall3 has been subjected to biaxial loading the FD graphs on each direction were plotted separately and compared to the experimental results. Exprimentally, The U-shaped wall failure, in both directions oocured at the apex of the large magnitude of the last fly (for a displacement value of 8cm in the X direction and -8cm in the Y direction), when three vertical bars broke straightening back up after buckling in compression. Then one flange failed in shear and a relative displacement of the top of the flange with respect to the bottom was observed. Based on a maximum displacement of 8cm and a yield displacement of about 1.3cm the available displacement ductility factor is approximately 6cm in both directions. From Figures 11(a)(b) and 12(a)(b), we see that there is a decrease in the capacity of the wall when it is subjected to bidirectional loading compared to unidirectional loading. This shows that due to the complex geometry of U-shape walls. There’s a decrease in its capacity when subjected to bi-directional loading.

CHAPTER 3

OBSERVATIONS AND DAMAGE STATE DETERMINATION.

After the reasonable validation between the simulated and experimental FD graphs for all the three walls from the previous chapter, we can conclude that VEEL is a valuable tool for understanding the seismic behavior of nonrectangular walls. To determine the level of damage with increasing peak drift value of the wall, contor plots (strain distribution plot) of YZ (web) and XZ (flanges) planes for Wall1 and Wall 2 were plotted. To systematically monitor the wall failure, we define two metrics 1) An area ratio of the wall surface that yielded (denoted as α). 2) An area ratio of the wall surface that undergoes crushing (denoted as β) to the entire wall area.

α: fraction of the wall surface which has undergone yielding, i.e. the ratio between the area of the surface where the strain value (ε) exceeds 0.002 in the contor plot to the total area of the wall surface.

β: fraction of the wall surface which has undergone crushing, i.e. the ratio between the area of the surface where the strain value (ε) is less than -0.002 in the contor plot to the total area of the wall surface.

We observed that rectangular surfaces of the U-shape wall could undergo by three types of damage patterns, which depends on the direction of loading

Type 1: When α fraction of the wall has yielded, as shown in Figure 13.

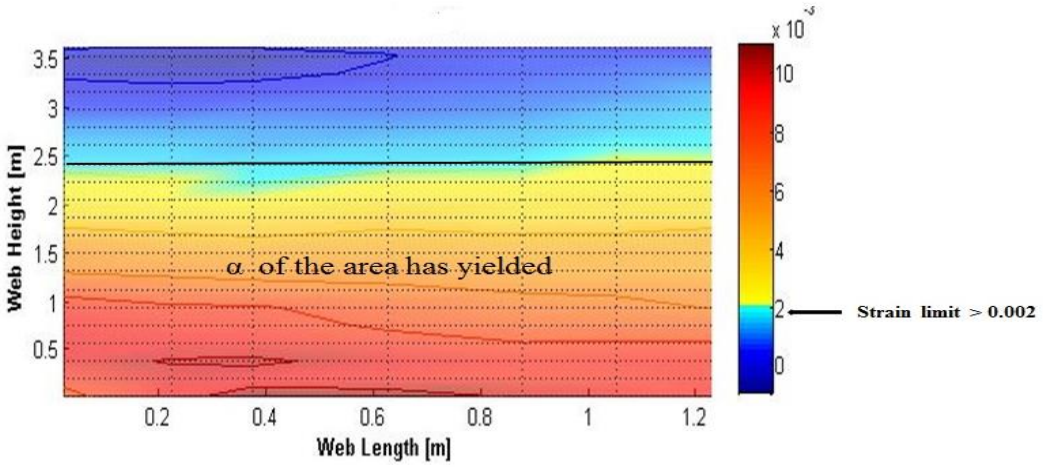

Figure 13: Contor plots- XZ plane of Wall1 at 2.05% drift ratio

Figure 13 contor plot is the XZ plane of Wall1 (i.e. loaded in the Y direction) at a positive peak displacement of 8cm at 60th-time step out of the 277-time steps.

Similarly for Wall2, the contor plot is the YZ plane of Wall2 (i.e. loaded in the X direction) at a positive peak displacement of 8cm at a time step of 153 out of the 220-time steps as shown in Figure 14.

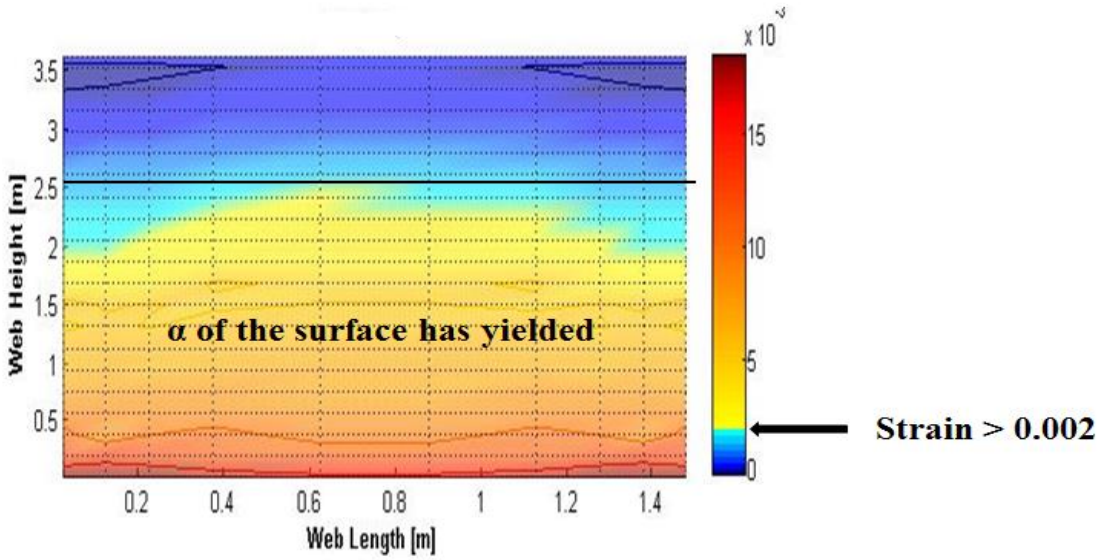

Figure 14: Contor plot- YZ plane of Wall2 at a drift of 2.05%

Type 2: When β fraction of the wall has crushed as shown in Figure 15.

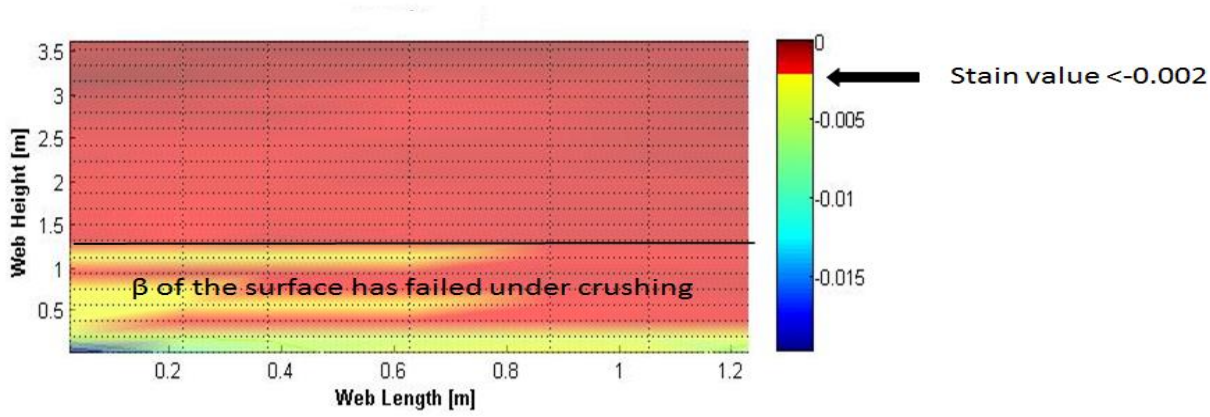

Figure 15: Contor Plot- XZ plane of Wall1 at a drift of 2.05%

Figure 15, contor plot is of XZ plane from Wall1 at a negative peak displacement of 4 cm and a time step of 48 out of the 268-time step.

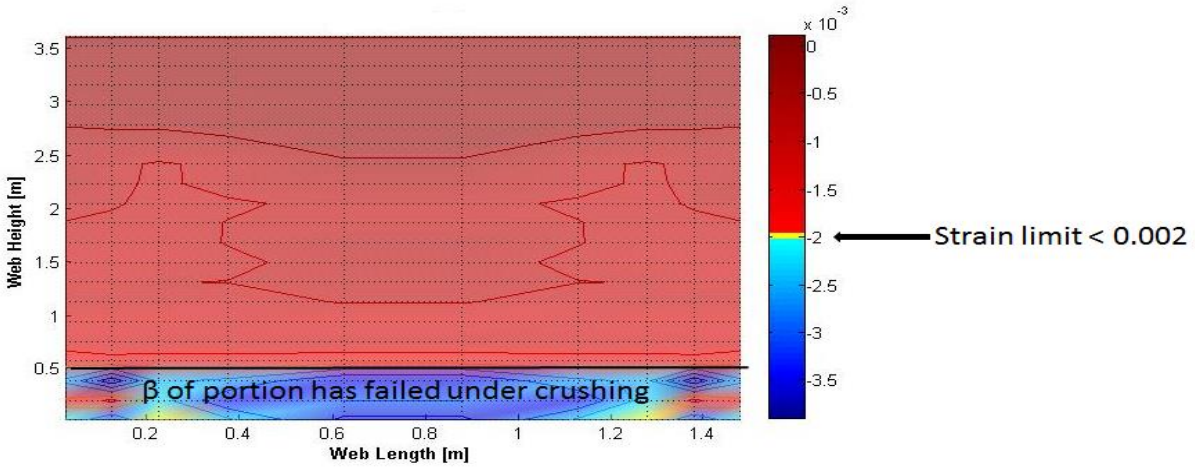

Figure 16: Contor plot – YZ plane of Wall2

Figure 16, contor plots is of YZ plane from Wall2 at a negative peak displacement of 4 cm and a time step of 81 out of the 220 time steps.

Type 3: When both α and β fraction of the surface has yielded and crushed

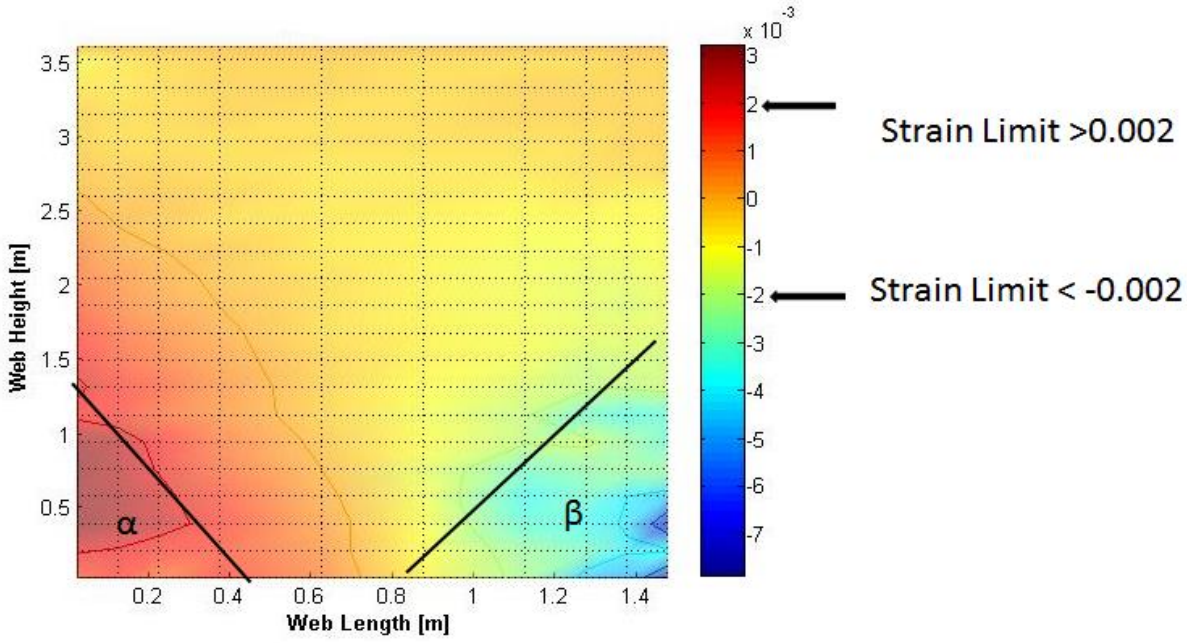

Figure 17: Contor plot- YZ plane of Wall1 at a drift equal to 2.05%

Figure 17, contor plot is of YZ plane from Wall1 at a positive peak displacement of 4cm and a time step equal to 40 out of the 268 whole time step.

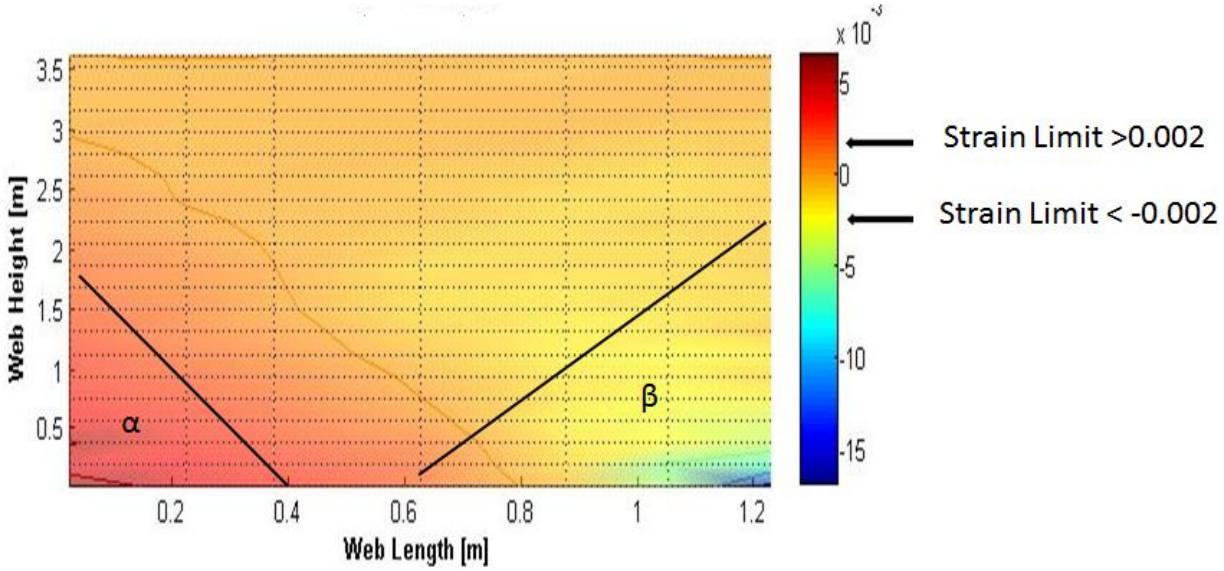

Figure 18: Contor plot- XZ plane of Wall2 at a drift equal to 1.03%

Figure 18, contor plot is of XZ plane of Wall2 at a positive peak displacement of 4 cm and a time step of 97 out of the 220-time steps.

Such contor plots have been plotted at every maximum peak displacement value (both in positive and negative direction) and variation of α and β is determined at every drift value for both XZ and YZ plane of Wall1 and Wall2.

1. **Wall1**

XZ plane: We observe only Type 1 and Type 2 damages to this surface, and the variation of α and β vs. drift ratio is shown in Figure 19:

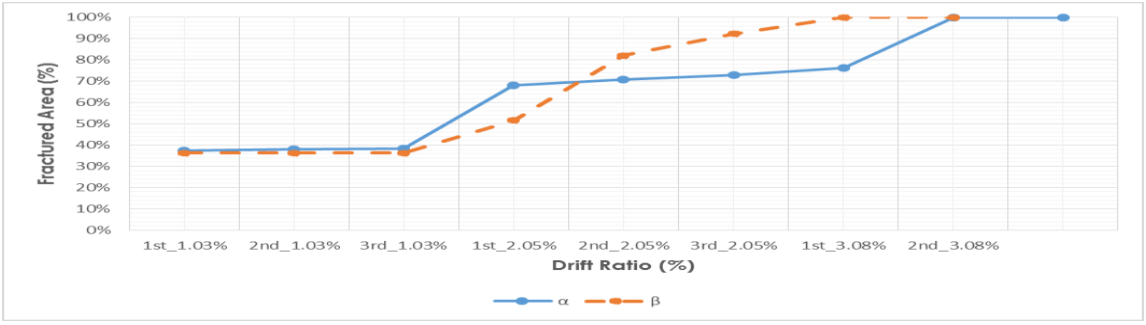

Figure 19: Variation of damage area with drift ratio for YZ plane – Wall1

YZ plane: We observe mostly Type 3 damage to the surface and the variation of α and β with drift ratio is shown in Figure 20(a) when the wall is under tension. We also determine the damage length and its variation with drift is shown in figure 20(b)

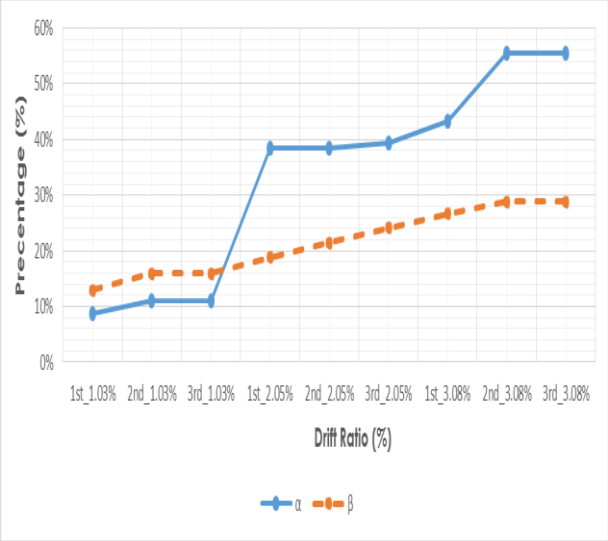

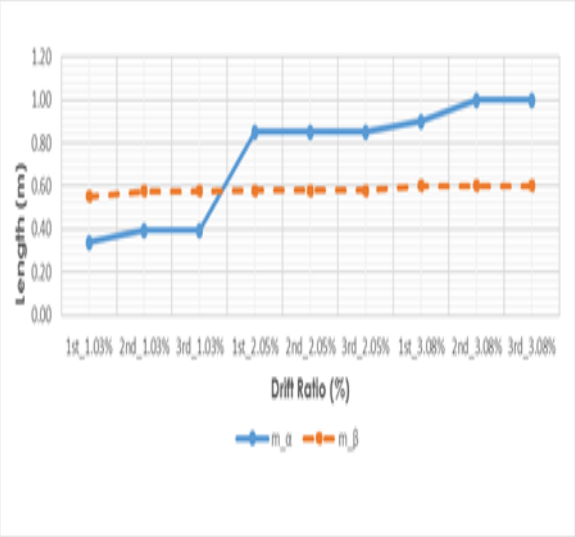

Figure 20 (a): Damage area vs. drift for YZ plane- Wall1 Figure 20 (b): Damage length for YZ plane- Wall1

Variation of damage area and length with drift ratio are shown in Figures 21, 22. When the wall is under Compression.

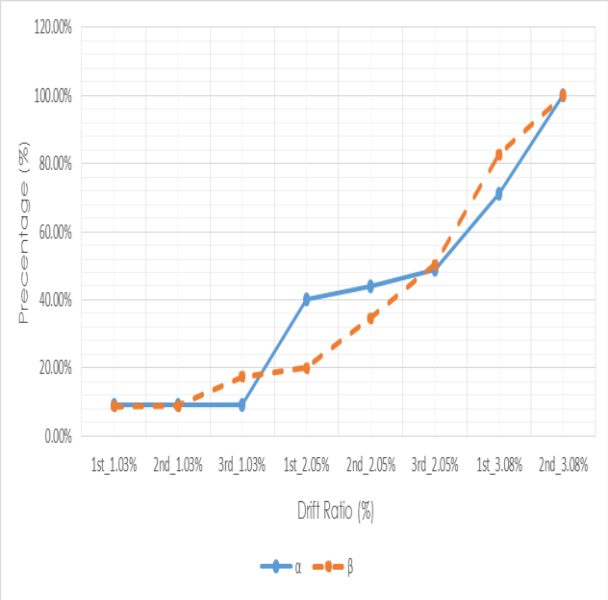

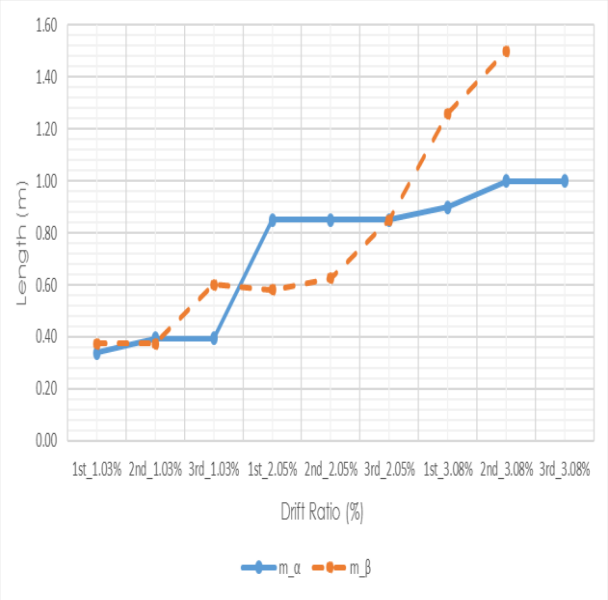

Figure 21: Damage area vs. Drift for YZ plane- Wall1 Figure 22: Damage length vs Drift for YZ plane

2. **Wall2**

XZ plane: We observe more Type 3 damage on the surface. The variation of α and β with drift are calculated and plotted in Figure 23(a) and 23(b).

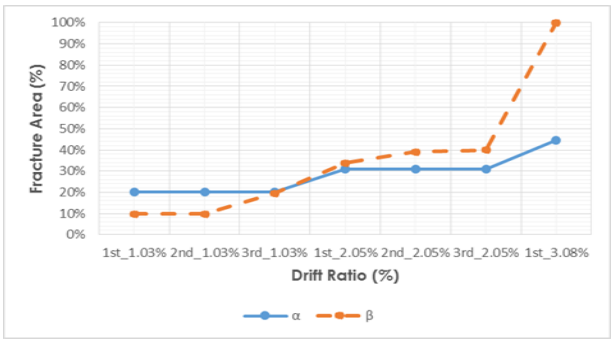

Figure 23(a): Damage area vs. drift for XZ plane

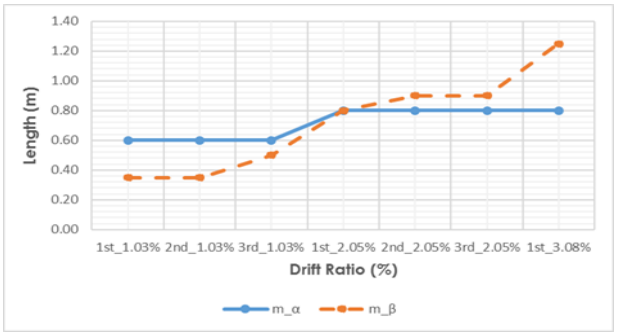

Figure 23(b): Damage length vs. drift for XZ

Variation of damage area and length with increase in drift, when wall is under compression

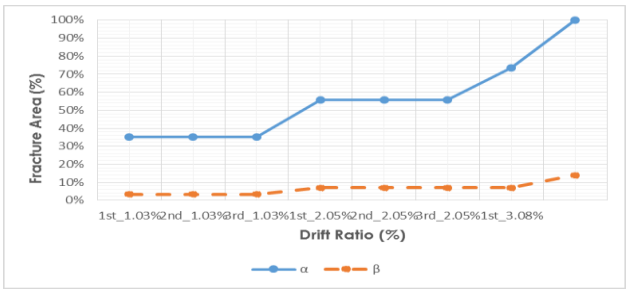

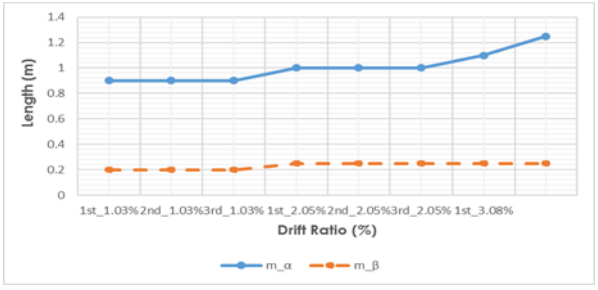

Figure 24: Damage area and length vs. drift ratio of Wall2-XZpalne under compression

YZ plane: We observe mostly Type 1 or Type 2 damage on this surface and the variation of α and β is shown in Figure 25.

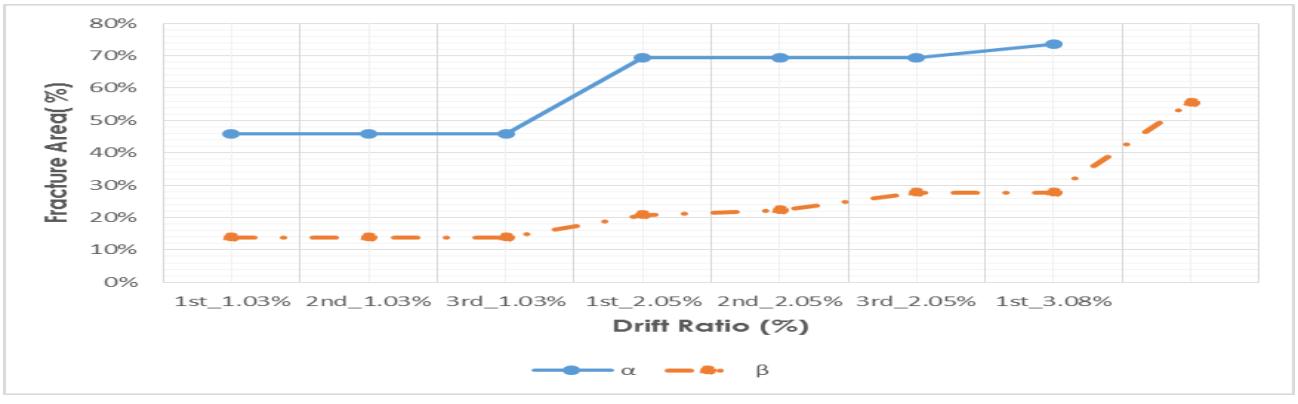

Figure 25: Variation of Damage Area with Drift Ratio for XZ plane

CHAPTER 4

FORMULATION OF STIFFNESS REDUCTION FACTOR.

4.1 Derivation of Stiffness reduction factor based on spring molecule

4.1.1 **Formulation for Uni-directional loading.**

In the spring molecule formulation, the entire wall surface is divided into m×n unit cells. Each unit cell comprises a nonlinear steel spring and a nonlinear compressive concrete spring with a compression-only gap (as shown in the figure 26). Initial stiffness for steel spring and concrete spring are K_s and K_c respectively, and they are connected in parallel, and the total initial stiffness is denoted as K_T.

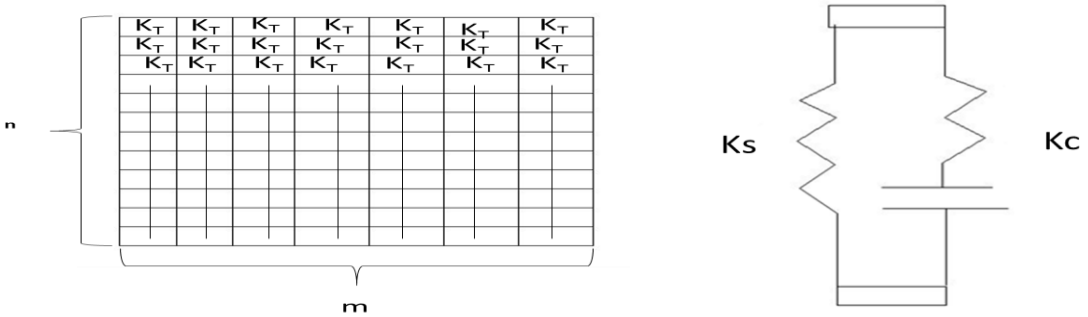

Figure 26: An mxn cell classification of the wall surface and a single spring molecule

Case 1: Total initial stiffness (K_o) of the wall is determined as follows:

$$K_T = K_s + K_c \delta_{gap}(\varepsilon) \qquad \text{Eq. 1}$$

where $K_s = \frac{\sigma_y}{\varepsilon_s}$, σ_y is the yield strength of boundary element vertical rebar inferred from [13] and ε_s is the yield strain of the rebar which is equal to 0.002

$K_c = \frac{\sigma_c}{\varepsilon_c}$, σ_c is the compressive strength of concrete inferred from [13] and ε_c is the compressive strain which is equal to -0.002 from figure 8(a); $\delta_{gap}(\varepsilon)$ is 1 when total strain of the cell $\varepsilon < 0$ while 0 when $\varepsilon \geq 0$. Thus, when the unit cell is under tension, $K_T = K_s$ whereas under compression $K_T = K_s + K_c$. If we consider one vertical row of unit cells (i.e. vertical chain of the n cells) there are n cells that are connected in series, hence for n springs in series, the effective

stiffness is equal to $K_{eff} = \frac{K_T}{n}$. Also, there are m columns of such cell chains in parallel (Fig. 26), and, thus the total initial stiffness is given by

$$K_o = \frac{m}{n} \times K_T \qquad \text{Eq. 2}$$

4.1.2 **Spring Molecule Constitutive Models**: The nonlinear behavior of the proposed spring molecule model derives entirely from the nonlinear behavior of the unit cells[4]. Thus the validity of the analytical results depends on the accuracy of the cell material models. Since the present study is focusing on the stiffness reduction of nonrectangular shear walls and the effect of bond-slip is neglected, only two material models are required, i.e., one for concrete and the other one for reinforcing steel.

4.1.2 (a): **Steel stress- strain relation**: The spring molecule model uses the bilinear model for reinforcing steel as described by Menegotto and Pinto [4]. The monotonic envelope curve of steel in compression and tension is shown in Figure 27.

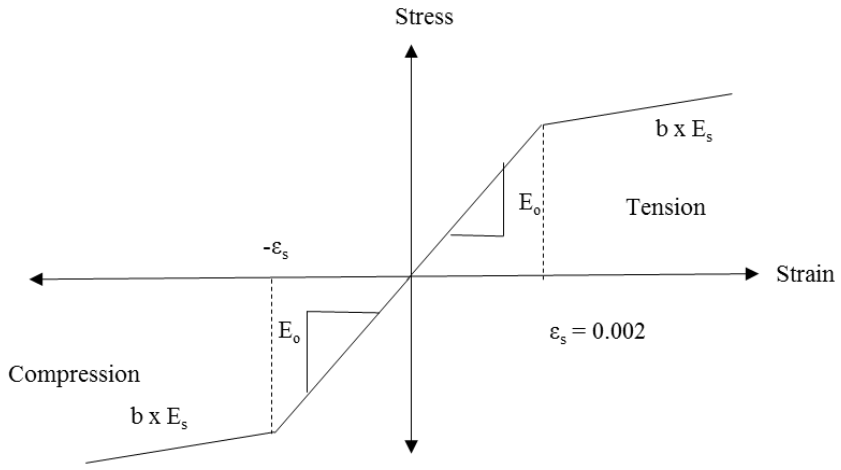

Figure 27: Bilinear model of reinforcing steel in spring molecule model

Where b is the steel stiffness reduction factor, and it is determined as the ratio between E_1 and E_O. E_O is the initial stiffness and E_1 is the slope of the line after yielding takes place, and throughout the present study b value is assumed to be 0.00156.

4.1.2 (b): **Concrete stress strain relation**: The monotonic envelope curve in compression follows the model of Kent and Park (1973) [4] that was later extended by *Scott et. al* (1982) [4]. Even though more accurate and complete models have been published since the so-called

modified Kent and Park model offers a good balance between simplicity[4] and accuracy. For confined concrete equations used are as follows [4]**.** The monotonic envelope curve is shown in figure 28.

$$\varepsilon_c \leq 0.002K\ ;\ \ \sigma_c = \ K \times f_c' \times \left[\frac{2\varepsilon_c}{0.002K} - \left(\frac{\varepsilon_c}{0.002K}\right)^2\right]$$

And when $\varepsilon_c > 0.002K\ ;\ \ \sigma_c = K \times f_c' \times [1 - Z(\varepsilon_c - 0.002K)]$

Where $Z = {0.5}\Big/\left(\frac{3+0.29f_c'}{145f_c'-1000} + \frac{3}{4}\rho_s\sqrt{\frac{h'}{s_h}} - 0.002K\right)$

$$\rho_s = \frac{Volume\ of\ Reinforcement\ in\ Stirrup}{Volume\ of\ confined\ concrete}$$

$$K = 1 + {\rho_s \times f_{yh}}\Big/{f_c'}$$

f_{ya} - The yield strength of the stirrup.

f_c' - The compressive strength of cylindrical concrete test specimen

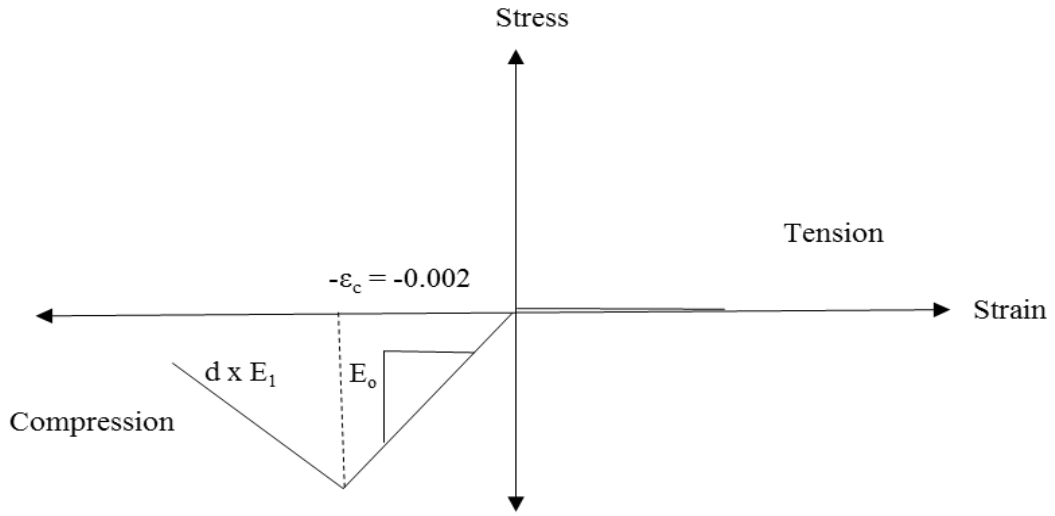

Figure 28: Monotonic envelope curve for concrete based on Kent and Park Model

Using the above equations, d – The stiffness reduction factor for concrete in compression is computed to be equal to -0.109322

Case2: Stiffness of wall when α fraction of the wall has horizontally yielded.

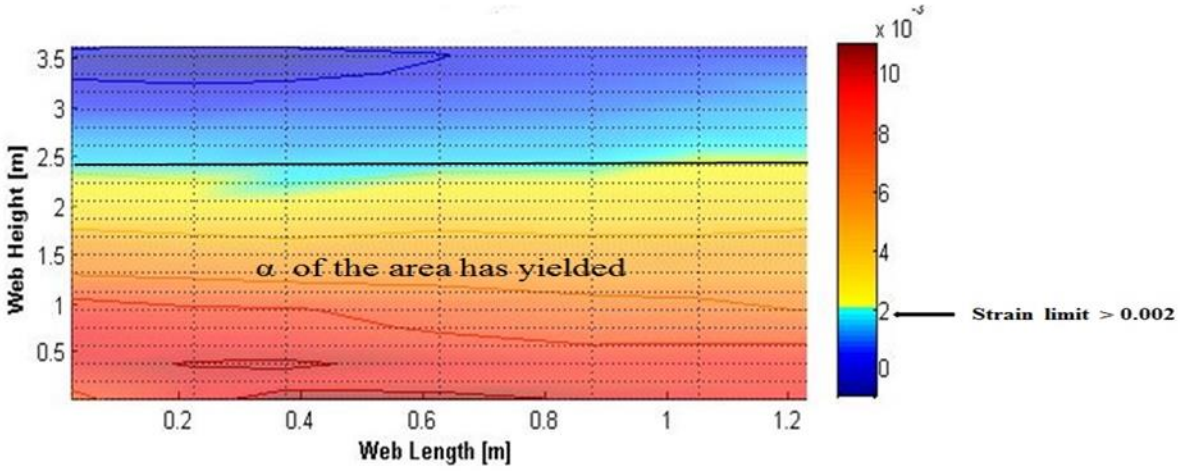

Figure 29: Type 1 damage state

All the cells which have undergone yielding will have a stiffness (K_{Ty}) which is determined as follows: As concrete is assumed to have no tensile stiffness, the *Kc* values be equal to zero under tension. Once nonlinearity starts the steel stiffness reduces from *Ks* to b**Ks*. Therefore, the new stiffness of those cells which have yielded comes out to be

$$K_{Ty} = b \times K_s \qquad \text{Eq. 3}$$

So, if α fraction of the n cells has yielded in a row of cell. Then we have n×α cells with a stiffness equal to K_{Ty} and (n- n×α) cells with stiffness equal to K_T. We can determine the stiffness for a single series as

$$\frac{1}{K} = \frac{n\alpha}{K_{Ty}} + \frac{n - n\alpha}{K_T}$$

By simplifying the above equation, we get

$$K = \left(\frac{1}{n}\right) \frac{K_{Ty} \times K_T}{\alpha K_T + (1-\alpha) K_{Ty}}$$

As there are m such rows of cells in parallel, the new stiffness of the wall after α fraction of it has yielded is given by

$$K = \frac{m}{n} \times \left(\frac{K_{Ty} \times K_T}{\alpha K_T + (1 - \alpha) K_{Ty}} \right) \quad \text{Eq. 4}$$

Case 3: when β fraction of the wall has undergone crushing

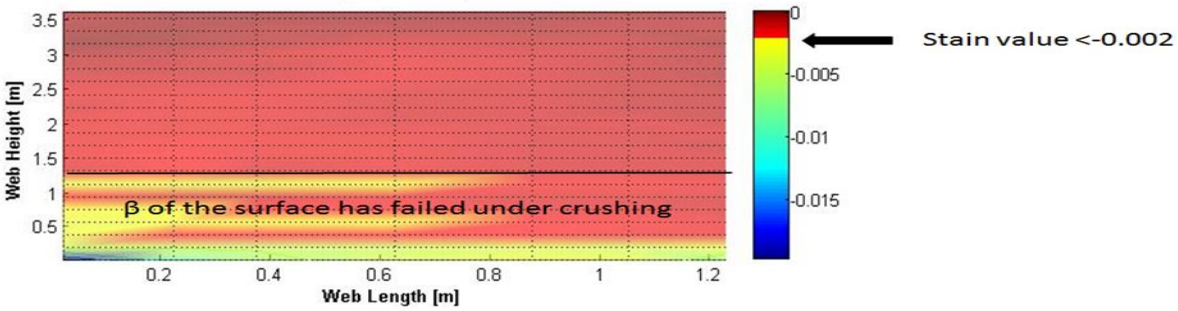

Figure 30: Type 2 damage state

All the cells which have undergone crushing will have a stiffness K_{TC} which is defined as follows. From the monotonic envelope curve for concrete model based on Kent and Park model, concrete stiffness reduced from K_C to d× K_C and the steel stiffness reduces from *Ks* to b×*Ks*. Therefore, the new stiffness of those cells which have crushed becomes

$$K_{Tc} = b \times K_s + d \times K_c \quad \text{Eq. 5}$$

So, if β fraction of the n cells has undergone concrete crushing. Then we have n×β cells with stiffness equal to K_{Tc}, and (n- n×β) cells with stiffness equal to K_T. We can determine the stiffness for a single series as

$$\frac{1}{K} = \frac{n\,\beta}{K_{Tc}} + \frac{n - n\,\beta}{K_T}$$

Simplifying the above equation by we get

$$K = \left(\frac{1}{n}\right) \frac{K_{TC} \times K_T}{\beta\, K_T + (1 - \beta\,) K_{TC}}$$

As there are m rows of cells in parallel, the new stiffness of the wall after β fraction of horizontal wall has crushed is given by

$$K = \frac{m}{n} \times \left(\frac{K_{TC} \times K_T}{\beta\, K_T + (1 - \beta) K_{TC}} \right) \qquad \text{Eq. 6}$$

Case 4: When α fraction of wall surface has yielded and simultaneously β fraction of the wall has undergone concrete crushing, as shown in Figure 31

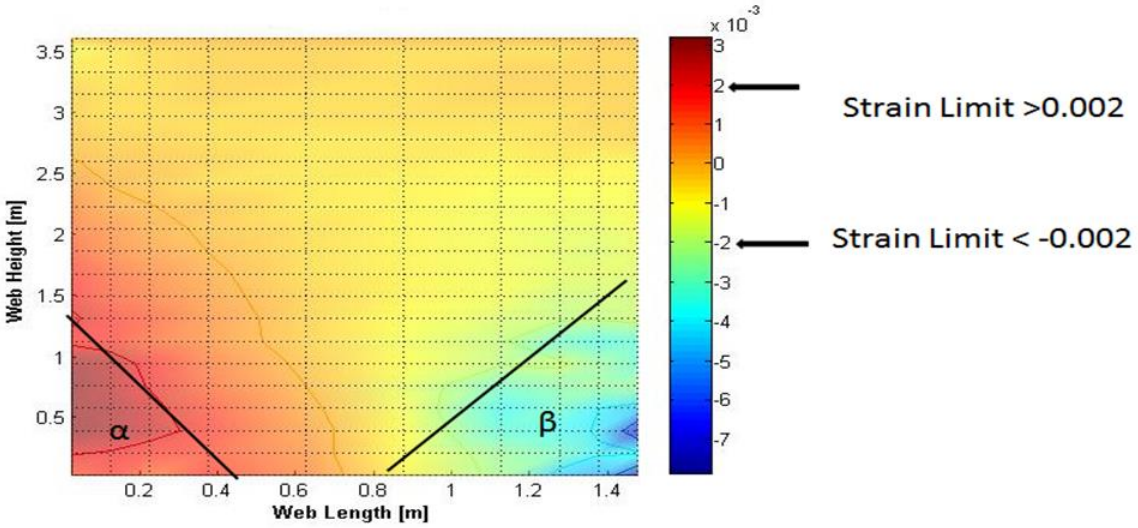

Figure 31: Type 3 damage state

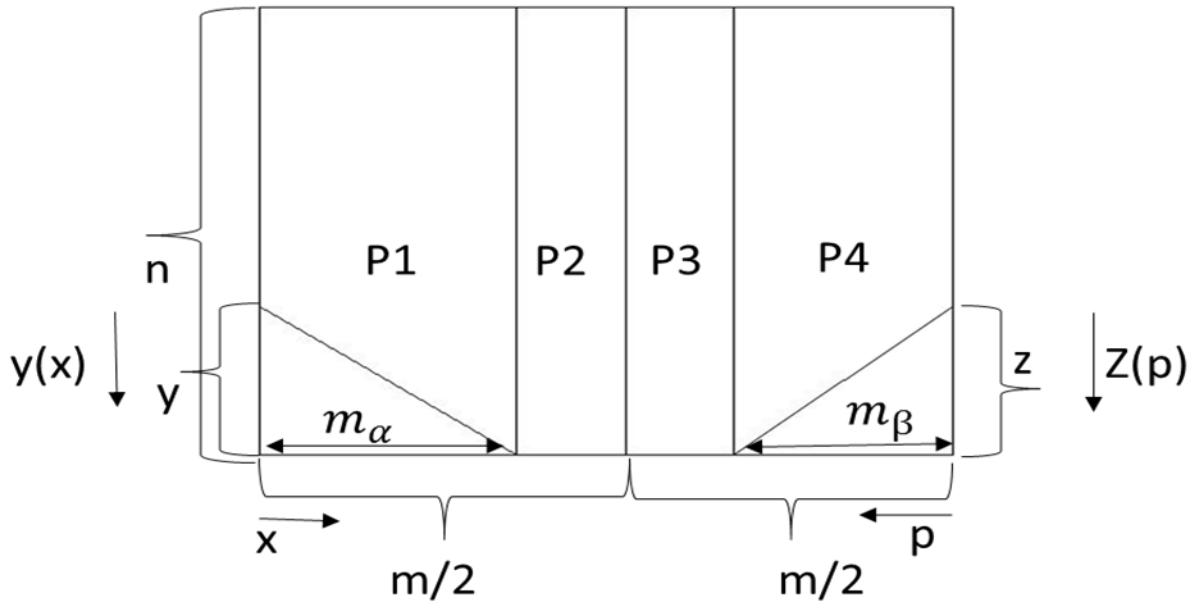

Figure 32: Dividing wall into parts for determining stiffness in case 4. P1 denoted Part 1.

To determine the stiffness in such a case, we first divide the wall into four sections as shown in Figure 32. We can collect the lengths (m_α *and* m_β) of damaged walls. The damage lengths may come from on-site observation or from the contour plots of simulation results. With increasing peak displacements, we can obtain varying damage lengths. It should be noted that in the above figure y and z are the number of cells in the vertical direction, whereas m_α and m_β are the lengths of yielding and crushing zones of the wall.

Let us consider Part 2 and Part 3 first, from the figure above we can say that none of the cells in the vertical direction have yielded nor crushed. Hence their stiffness is equal to K_T. There are n cells with stiffness K_T connected in series. Hence the stiffness for a single vertical series in that region is equal to $\frac{K_T}{n}$. For Part 2, number of effective springs connected in parallel are ($m/2 - m_\alpha$). Therefore, the total stiffness (K_{P2}) for Part 2 is given by

$$K_{P2} = \frac{\frac{m}{2} - m_\alpha}{n} \times K_T \qquad \text{Eq. 7}$$

Similarly, for Part 3 we can find the stiffness to be equal to

$$K_{P3} = \frac{\frac{m}{2} - m_\beta}{n} \times K_T \qquad \text{Eq. 8}$$

Part 1:

By recalling that α is the area ratio of the yielded zone to the entire wall, we can consider area equality of the yielded triangle as $\frac{1}{2} \times m_\alpha \times y = \alpha \times m \times n$. From this, we can determine the only unknown quantity

$$y = \frac{2\alpha mn}{m_\alpha}$$

We observe that the y value (i.e. number of vertical unit cells that are yielding) keeps decreasing as we move from left to right. Hence y value in terms of x can be written as follows

$$y(x) = \frac{2\alpha mn}{m_\alpha^2}(m_\alpha - x)$$

where the number of horizontal cells, x ranges from 0 to m_α. In a vertical row of unit cells, y (x)

cells will have a stiffness equal to K_{Ty} and (n-y(x)) cells have a stiffness equal to K_T. Hence the stiffness for a single series of cells can be determined as

$$\frac{1}{K} = \frac{y(x)}{K_{Ty}} + \frac{n - y(x)}{K_T}$$

By simplifying the above equation, we get

$$K = \frac{K_T \times K_{Ty}}{(n - y(x))K_{Ty} + y(x)K_T}$$

However, we know that y is a function of x. Hence the total stiffness of part 1 is given by

$$K_{P1} = \sum_{x=0}^{x=m_\alpha} \frac{K_T \times K_{Ty}}{[n - y(x)]K_{Ty} + y(x)K_T} \qquad \text{Eq. 9}$$

Similarly, for Part 4, same procedure can be followed as Part 1 and we can determine the total stiffness as

$$K_{P4} = \sum_{p=0}^{p=m_\beta} \frac{K_T \times K_{TC}}{[n - Z(p)]K_{TC} + Z(p)K_T} \qquad \text{Eq. 10}$$

where, $Z(p) = \frac{2\beta mn}{m_\beta^2}\left(m_\beta - p\right)$ where p is the horizontal coordinate (measured from the right corner) meaning the counts of horizontal cells.

Therefore, the total stiffness (K) is given by

$$K = K_{p1} + K_{p2} + K_{p3} + K_{p4} \qquad \text{Eq. 11}$$

4.2 **Formulation for bi-directional loading**.

In the bi-directional loading case, the wall has been displaced to the maximum point in one direction, and then it is loaded in the other direction (e.g. loaded in X direction and then Y-direction). Hence the damage patterns on the web and flange of the wall are complex. These complex damage patterns can be divided into several cases based on a number of assumptions in this study. Then an analytical stiffness reduction formula is derived for each case.

4.2.1 Damage patterns observed on the web portion of the wall due to bi-directional loading.

Suppose, a wall is initially loaded in the X direction (i.e., parallel to two flanges). Hence we observe Type1 or Type 2 damage pattern on the web surface. Once, the direction of the loading is changed to the Y direction we start observing Type3 damage pattern over the current damaged surface as shown in figure 33 and figure 37

4.2.1(a) **Stiffness reduction formulae when Type 1 damage is observed due to X direction loading**

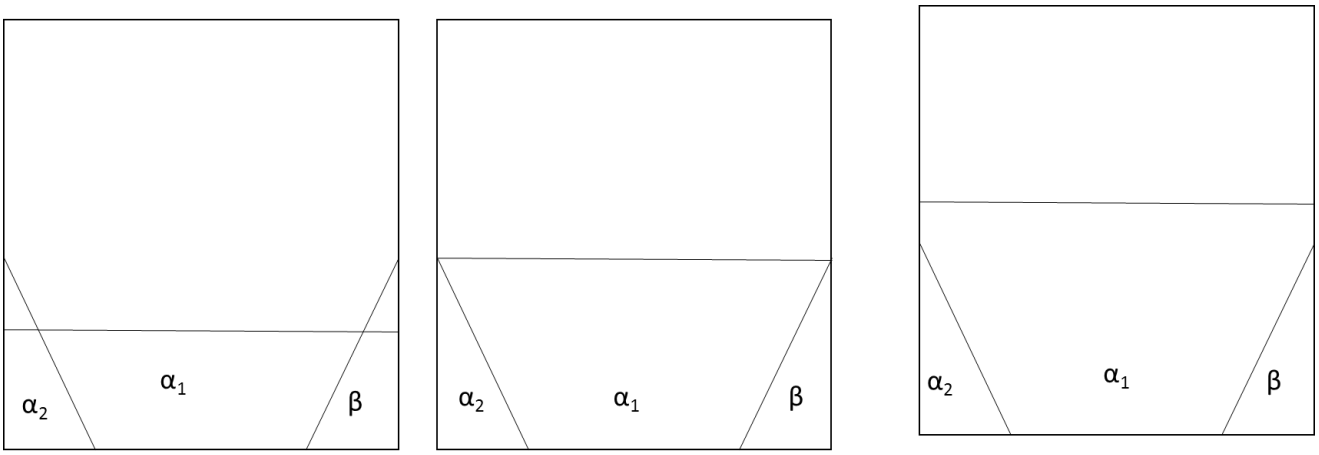

Figure 33: All possible damage patterns on the web surface of the wall by changing the direction of loading. X-direction loading causes α_1, which is followed by α_2 and β from Y- direction loading

a) Case 1: when $h_{\alpha 1} < h_{\alpha 2}$ *and* $h_{\alpha 1} < h_{\beta}$

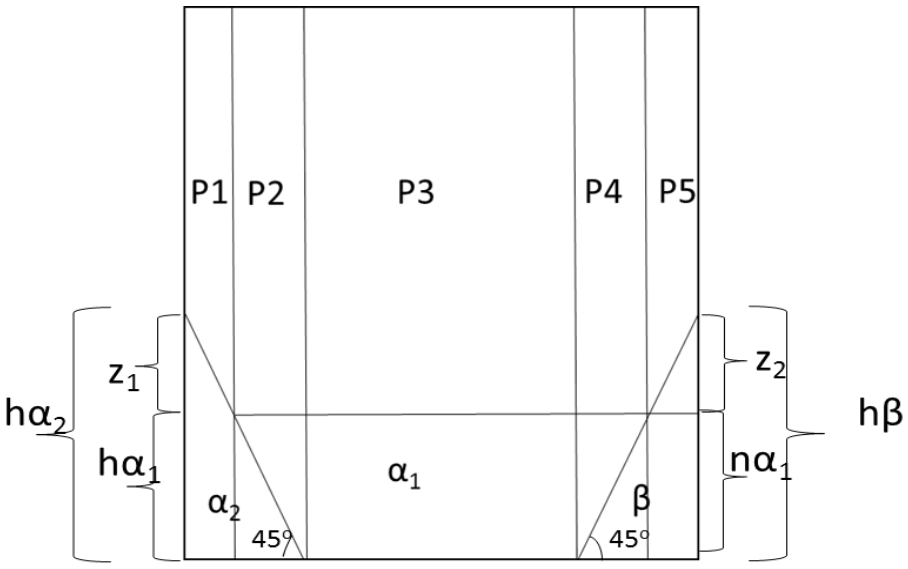

Figure 34: Case 1 when $h_{\alpha 1} < h_{\alpha 2}$ and $h_{\alpha 1} < h_{\beta}$

The stiffness (K) for such a wall surface is determined by dividing the wall surface into five parts as shown in figure 34. The total stiffness of the wall surface would be the sum of all the parts. For simplicity, we assumed a 45^o angle damage for damage α_2 and β.

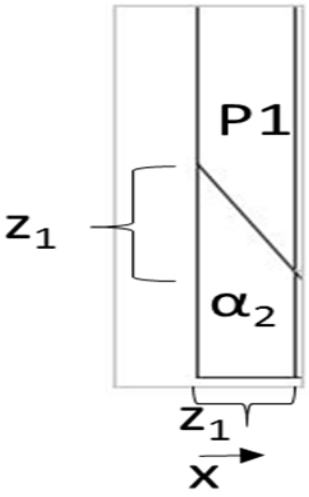

Figure 34 (a): Part 1

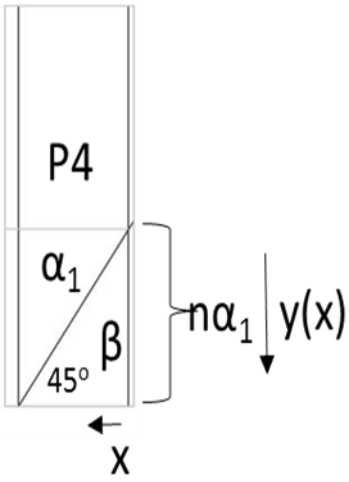

Figure 34(b): Part 4

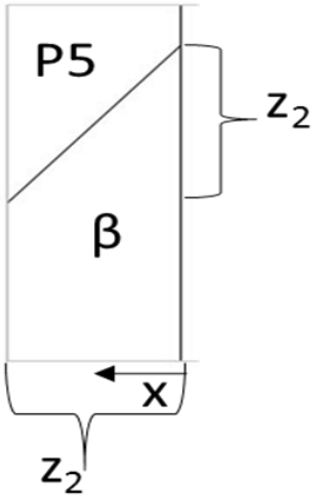

Figure 34(c): Part5

For Part 1:

$$K_{P1} = \sum_{x=0}^{x=z_1} \frac{K_T \times K_{Ty}}{[n - y(x)]K_{Ty} + y(x)K_T} \qquad \text{Eq. 12}$$

where $z_1 = \sqrt{2\times\alpha_2\times m\times n} - (n\times\alpha_1)$ and $y(x) = \sqrt{2\times\alpha_2\times m\times n} - x$

For Part2:

$$K_{P2} = \frac{\sqrt{2\times\alpha_2\times m\times n} - z_1}{n} \times \left(\frac{K_{Ty}\times K_T}{\alpha_1 K_T + (1 - \alpha_1)K_{Ty}}\right) \qquad \text{Eq. 13}$$

For Part3:

$$K_{P3} = \frac{m - \sqrt{2\times\alpha_2\times m\times n} - \sqrt{2\times\beta\times m\times n}}{n} \times \left(\frac{K_{Ty}\times K_T}{\alpha_1 K_T + (1 - \alpha_1)K_{Ty}}\right) \qquad \text{Eq. 14}$$

For Part4:

As you can see from Figures 34 and 34 (b), the y value keeps decreasing as we move from right to left. Hence y value in terms of x can be written as follows

$$y(x) = n\times\alpha_1 - x$$

where the number of horizontal cells, x ranges from 0 to $\sqrt{2\times\beta\times m\times n} - z_2$. In a vertical row of unit cells, y (x) cells will have a stiffness equal to K_{Tc} and (n×α_1 – y (x)) cells will have a stiffness equal to K_{Ty} and (n- n×α_1) cells have a stiffness equal to K_T. Hence the stiffness for a single series of cells can be determined as

$$\frac{1}{K} = \frac{y(x)}{K_{Tc}} + \frac{n\times\alpha_1 - y(x)}{K_{Ty}} + \frac{n - n\times\alpha_1}{K_T}$$

By simplifying the above equation, we get

$$K_{P4} = \sum_{x=0}^{x=\sqrt{2\times\beta\times m\times n}-z_2} \frac{K_T\times K_{Ty}\times K_{Tc}}{[n\times\alpha_1 - y(x)]K_T K_{Tc} + y(x)K_T K_{Ty} + (n - n\times\alpha_1)K_{Ty}K_{Tc}} \quad \text{Eq. 15}$$

where $z_2 = \sqrt{2\times\beta\times m\times n} - (n\times\alpha_1)$ and $y(x) = n\times\alpha_1 - x$

For Part5:

$$K_{P5} = \sum_{x=0}^{x=z_2} \frac{K_T\times K_{Tc}}{[n - y(x)]K_{Tc} + y(x)K_T} \quad \text{Eq. 16}$$

where $z_2 = \sqrt{2\times\beta\times m\times n} - (n\times\alpha_1)$ and $y(x) = \sqrt{2\times\beta\times m\times n} - x$

Therefore, the overall stiffness of the wall surface

$$K = K_{P1} + K_{P2} + K_{P3} + K_{P4} + K_{P5} \quad \text{Eq. 17}$$

Case 2: when $h_{\alpha 1} = h_{\alpha 2}$ *and* $h_{\alpha 1} = h_\beta$

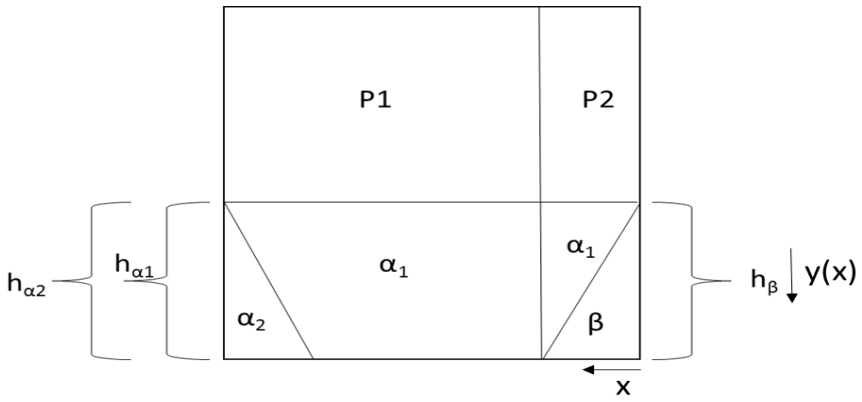

Figure 35: when $h_{\alpha 1} = h_{\alpha 2}$ and $h_{\alpha 1} = h_\beta$

As you can see from the figure 35, we divide the wall into two parts. The overall stiffness of the wall is the summation of the two parts. Note we have assumed a 45^o angle damage for β

For Part 1

$$K_{P1} = \frac{m - \sqrt{2\times\beta\times m\times n}}{n} \times \left(\frac{K_{Ty}\times K_T}{\alpha_1 K_T + (1 - \alpha_1)K_{Ty}} \right) \quad \text{Eq. 18}$$

For Part 2

As you can see from Figures 35, the y value keeps decreasing as we move from right to left. Hence y value in terms of x can be written as follows

$$y(x) = n\times\alpha_1 - x$$

where the number of horizontal cells, x ranges from 0 to $\sqrt{2\times\beta\times m\times n}$. In a vertical row of unit cells, y (x) cells will have a stiffness equal to K_{Tc} and (n×α$_1$ – y (x)) cells will have a stiffness equal to K_{Ty} and (n- n×α$_1$) cells have a stiffness equal to K_T. Hence the stiffness for a single series of cells can be determined as

$$\frac{1}{K} = \frac{y(x)}{K_{Tc}} + \frac{n\times\alpha_1 - y(x)}{K_{Ty}} + \frac{n - n\times\alpha_1}{K_T}$$

By simplifying the above equation, we get

$$K_{P2} = \sum_{x=0}^{x=\sqrt{2\times\beta\times m\times n}} \frac{K_T\times K_{Ty}\times K_{Tc}}{[n\times\alpha_1 - y(x)]K_T K_{Tc} + y(x)K_T K_{Ty} + (n - n\times\alpha_1)K_{Ty}K_{Tc}} \quad \text{Eq. 19}$$

The overall stiffness of the wall is given by $K = K_{P1} + K_{P2}$ Eq. 20

Case 3: when $h_{\alpha 1} > h_{\alpha 2}$ *and* $h_{\alpha 1} > h_{\beta 1}$

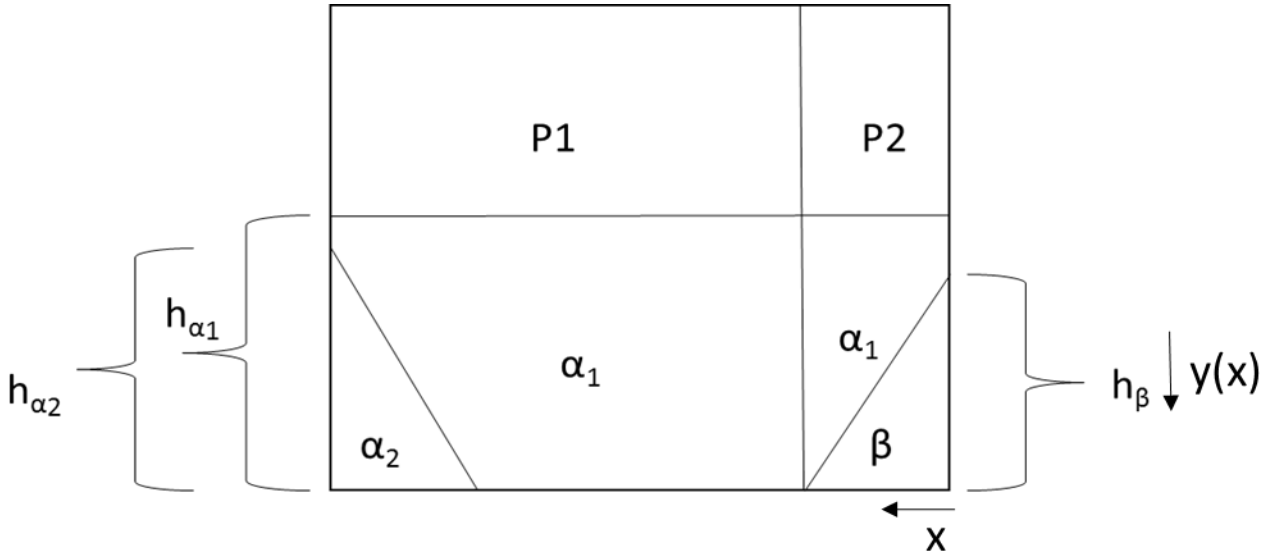

Figure 36: Case 3: $h_{\alpha 1} > h_{\alpha 2}$ and $h_{\alpha 1} > h_{\beta}$

As you can see from the figure 36, we divide the wall into two parts. The overall stiffness of the wall is the summation of the two parts. Note we have assumed a 45° angle damage for α_2 and β

Part 1:

$$K_{P1} = \frac{m - \sqrt{2\times\beta\times m\times n}}{n} \times \left(\frac{K_{Ty}\times K_T}{\alpha_1 K_T + (1 - \alpha_1) K_{Ty}} \right) \qquad \text{Eq. 21}$$

For Part 2

As you can see from Figures 36, the y value keeps decreasing as we move from right to left. Hence y value in terms of x can be written as follows

$$y(x) = \sqrt{2\times\beta\times m\times n} - x$$

where the number of horizontal cells, x ranges from 0 to $\sqrt{2\times\beta\times m\times n}$. In a vertical row of unit cells, y (x) cells will have a stiffness equal to K_{Tc} and (n×α_1 – y (x)) cells will have a stiffness equal to K_{Ty} and (n- n×α_1) cells have a stiffness equal to K_T. Hence the stiffness for a single series of cells can be determined as

$$\frac{1}{K} = \frac{y(x)}{K_{Tc}} + \frac{n\times\alpha_1 - y(x)}{K_{Ty}} + \frac{n - n\times\alpha_1}{K_T}$$

By simplifying the above equation, we get

$$K_{P2} = \sum_{x=0}^{x=\sqrt{2\times\beta\times m\times n}} \frac{K_T \times K_{Ty} \times K_{Tc}}{[n\times\alpha_1 - y(x)]K_T K_{Tc} + y(x)K_T K_{Ty} + (n - n\times\alpha_1)K_{Ty}K_{Tc}} \quad \text{Eq. 22}$$

The overall stiffness of the wall is given by $K = K_{P1} + K_{P2}$ Eq. 23

4.2.1 (b) **Stiffness reduction formulae when Type 2 damage is observed due to X direction loading**

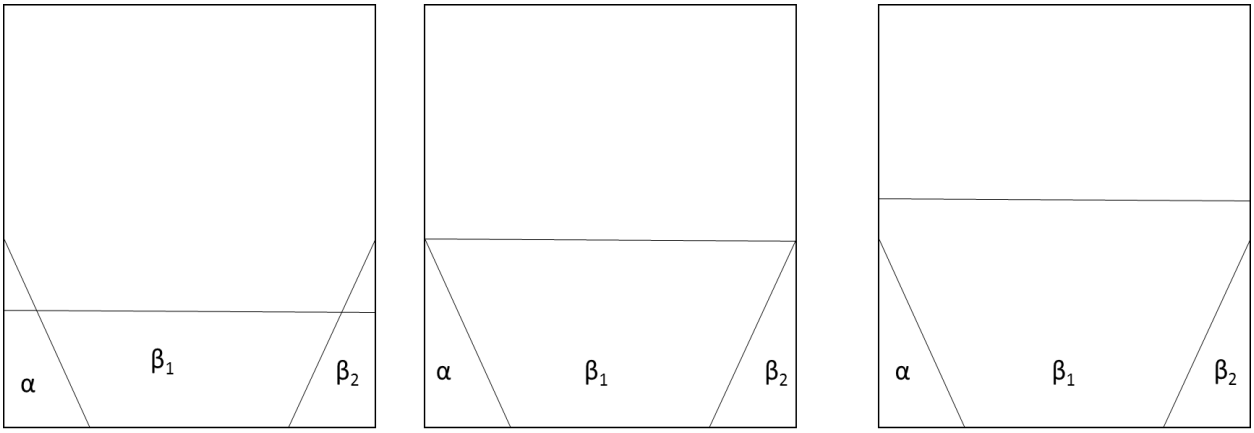

Figure 37: All possible damage patterns on the web surface of the wall by changing the direction of loading. X-direction loading causes β_1, which is followed by α and β_1 from Y- direction loading

a) Case 1: when $h_{\beta1} < h_{\beta2}$ and $h_{\beta1} < h_{\alpha}$

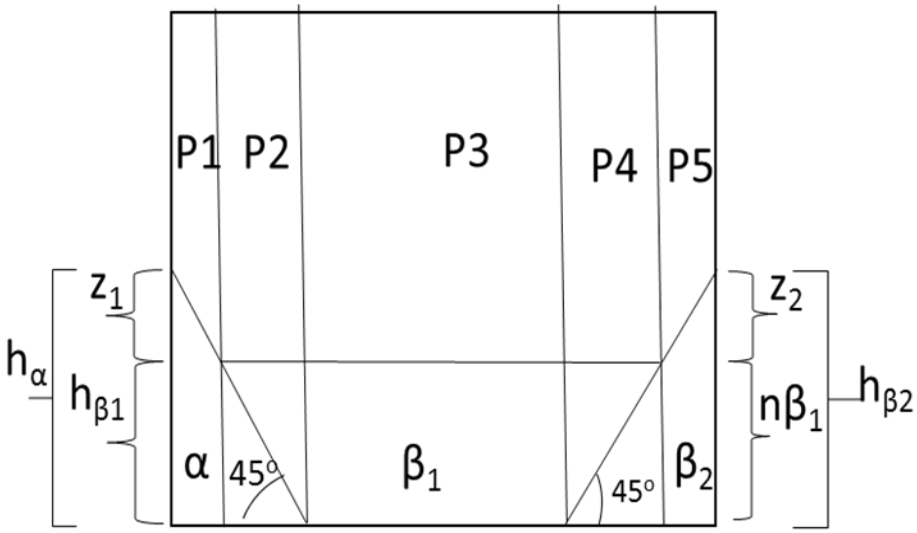

Figure 38: Case 1 when $h_{\beta1} < h_{\beta2}$ *and* $h_{\beta1} < h_{\alpha}$

The stiffness (K) for such a wall surface is determined by dividing the wall surface into five parts as shown in figure 34. The total stiffness of the wall surface would be the sum of all the parts. For simplicity, we assumed a 45^o angle damage for damage α and β_2.

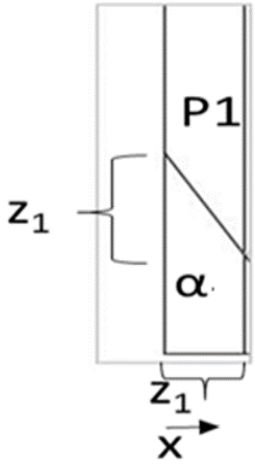

Figure 38 (a): Part 1

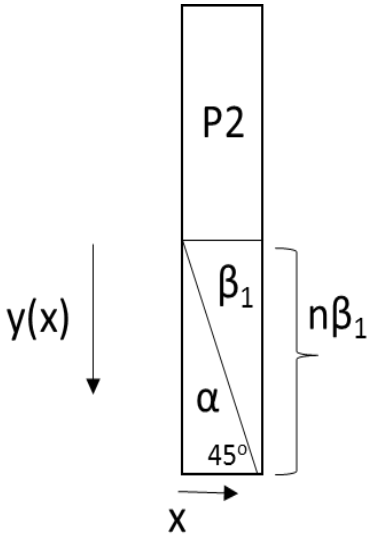

Figure 38(b): Part 2

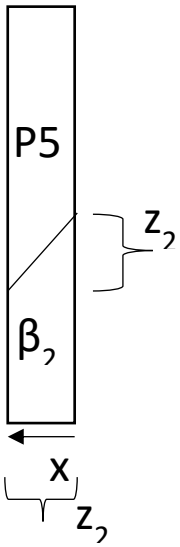

Figure 38(c): Part5

For Part 1:

$$K_{P1} = \sum_{x=0}^{x=z_1} \frac{K_T \times K_{Ty}}{[n - y(x)]K_{Ty} + y(x)K_T} \qquad \text{Eq. 24}$$

Where $z_1 = \sqrt{2\times\alpha\times m\times n} - (n\times\beta_1)$ and $y(x) = \sqrt{2\times\alpha\times m\times n} - x$

For Part2:

As you can see from Figure 38 and 38(b), the y value keeps decreasing as we move from left to right. Hence y value in terms of x can be written as follows

$$y(x) = n\times\beta_1 - x$$

where the number of horizontal cells, x ranges from 0 to $\sqrt{2\times\alpha\times m\times n} - z_1$. In a vertical row of unit cells, y(x) cells will have a stiffness equal to K_{Ty} and $n\times\beta_1 - y(x)$ cells will have a stiffness equal to K_{Tc} and (n- n$\times\beta_1$) cells will have a stiffness equal to K_T. Hence the stiffness for a single series of cells can be determined as

$$\frac{1}{K} = \frac{y(x)}{K_{Ty}} + \frac{n\times\beta_1 - y(x)}{K_{Tc}} + \frac{n - n\times\beta_1}{K_T}$$

By simplifying the above equation, we get

$$K_{P2} = \sum_{x=0}^{x=\sqrt{2\times\alpha\times m\times n}-z_1} \frac{K_T\times K_{Ty}\times K_{Tc}}{[n\times\beta_1 - y(x)]K_T K_{Ty} + y(x)K_T K_{Tc} + (n - n\times\beta_1)K_{Ty}K_{Tc}} \quad \text{Eq. 25}$$

Where $z_1 = \sqrt{2\times\alpha\times m\times n} - (n\times\beta_1)$ and $y(x) = n\times\beta_1 - x$

For Part3:

$$K_{P3} = \frac{m - \sqrt{2\times\beta_2\times m\times n} - \sqrt{2\times\alpha\times m\times n}}{n} \times \left(\frac{K_{Tc}\times K_T}{\beta_1 K_T + (1 - \beta_1)K_{Tc}}\right) \quad \text{Eq. 26}$$

For Part4:

$$K_{P4} = \frac{\sqrt{2\times\beta_2\times m\times n} - z_2}{n} \times \left(\frac{K_{Tc}\times K_T}{\beta_1 K_T + (1 - \beta_1)K_{Tc}}\right) \quad \text{Eq. 27}$$

where $z_2 = \sqrt{2\times\beta_2\times m\times n} - (n\times\beta_1)$.

For Part5:

$$K_{P5} = \sum_{x=0}^{x=z_2} \frac{K_T\times K_{Tc}}{[n - y(x)]K_{Tc} + y(x)K_T} \quad \text{Eq. 28}$$

Where $z_2 = \sqrt{2\times\beta_2\times m\times n} - (n\times\beta_1)$ and $y(x) = \sqrt{2\times\beta_2\times m\times n} - x$

Therefore, the overall stiffness of the wall surface

$$K = K_{P1} + K_{P2} + K_{P3} + K_{P4} + K_{P5} \quad \text{Eq. 29}$$

Case 2: when $h_{\beta 1} = h_{\beta 2}$ *and* $h_{\alpha} = h_{\beta 1}$

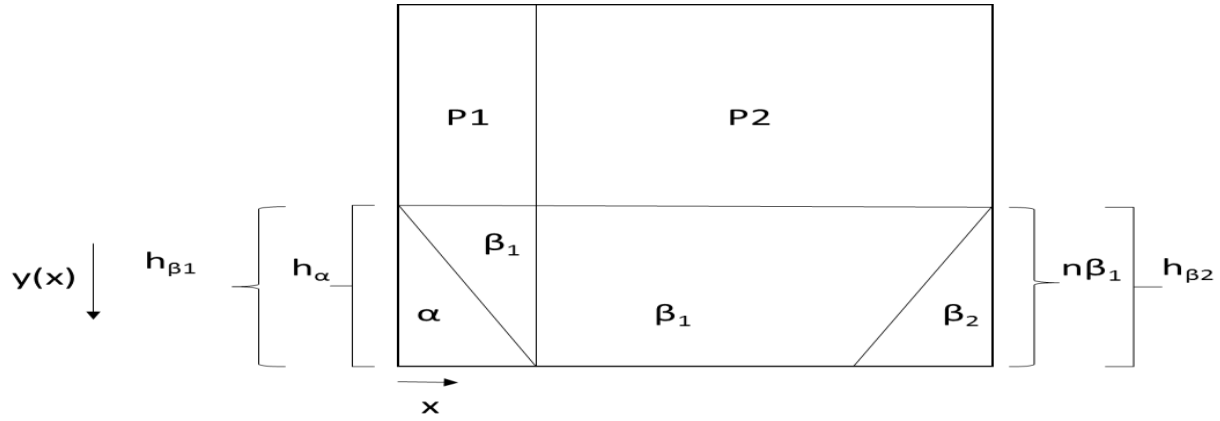

Figure 39: when $h_{\beta 1} = h_{\beta 2}$ and $h_{\alpha} = h_{\beta 1}$

As you can see from the figure 39, we divide the wall into two parts. The overall stiffness of the wall is the summation of the two parts. Note we have assumed a 45° angle damage for α and β_2

For Part 1

As you can see from Figure 39, the y value keeps decreasing as we move from left to right. Hence y value in terms of x can be written as follows

$$y(x) = n \times \beta_1 - x$$

where the number of horizontal cells, x ranges from 0 to $\sqrt{2 \times \alpha \times m \times n}$. In a vertical row of unit cells, y(x) cells will have a stiffness equal to K_{Ty} and $n \times \beta_1 - y(x)$ cells will have a stiffness equal to K_{Tc} and (n- $n \times \beta_1$) cells will have a stiffness equal to K_T. Hence the stiffness for a single series of cells can be determined as

$$\frac{1}{K} = \frac{y(x)}{K_{Ty}} + \frac{n \times \beta_1 - y(x)}{K_{Tc}} + \frac{n - n \times \beta_1}{K_T}$$

By simplifying the above equation, we get

$$K_{P2} = \sum_{x=0}^{x=\sqrt{2 \times \alpha \times m \times n}} \frac{K_T \times K_{Ty} \times K_{Tc}}{[n \times \beta_1 - y(x)] K_T K_{Ty} + y(x) K_T K_{Tc} + (n - n \times \beta_1) K_{Ty} K_{Tc}} \qquad \text{Eq. 30}$$

For Part 2:

$$K_{P3} = \frac{m - \sqrt{2\times\alpha\times m\times n}}{n} \times \left(\frac{K_{Tc}\times K_T}{\beta_1 K_T + (1 - \beta_1)K_{Tc}}\right) \quad \text{Eq. 31}$$

The overall stiffness of the wall given by $K = K_{P1} + K_{P2}$ Eq. 32

Case 3: when $h_{\beta 1} > h_{\beta 2}$ *and* $h_{\beta 1} > h_{\alpha}$

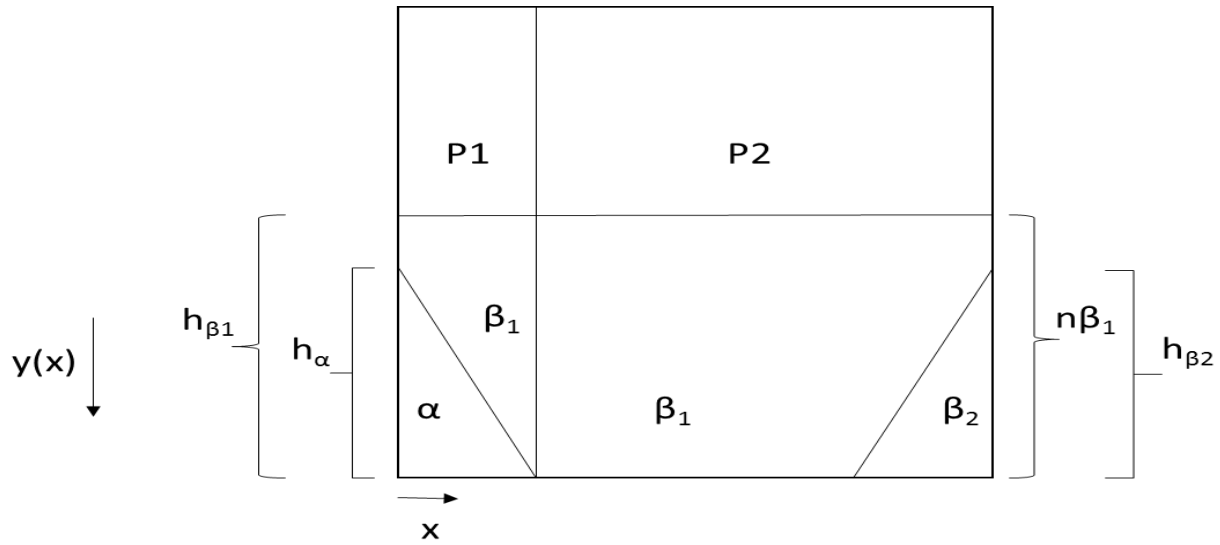

Figure 40: Case 3: $h_{\beta 1} > h_{\beta 2}$ and $h_{\beta 1} > h_{\alpha}$

As you can see from the figure 40, we divide the wall into two parts. The overall stiffness of the wall is the summation of the two parts. Note we have assumed a 45° angle damage for α and β_2

For Part 1:

As you can see from Figure 40, the y value keeps decreasing as we move from left to right. Hence y value in terms of x can be written as follows

$$y(x) = n\times\beta_1 - x$$

where the number of horizontal cells, x ranges from 0 to $\sqrt{2\times\alpha\times m\times n}$. In a vertical row of unit cells, y(x) cells will have a stiffness equal to K_{Ty} and $n\times\beta_1 - y(x)$ cells will have a stiffness equal to K_{Tc} and (n- n×β_1) cells will have a stiffness equal to K_T. Hence the stiffness for a single series of cells can be determined as

$$\frac{1}{K} = \frac{y(x)}{K_{Ty}} + \frac{n \times \beta_1 - y(x)}{K_{Tc}} + \frac{n - n \times \beta_1}{K_T}$$

By simplifying the above equation, we get

$$K_{P1} = \sum_{x=0}^{x=\sqrt{2 \times \alpha \times m \times n}} \frac{K_T \times K_{Ty} \times K_{Tc}}{[n \times \beta_1 - y(x)] K_T K_{Ty} + y(x) K_T K_{Tc} + (n - n \times \beta_1) K_{Ty} K_{Tc}} \quad \text{Eq. 33}$$

For Part 2:

$$K_{P3} = \frac{m - \sqrt{2 \times \alpha \times m \times n}}{n} \times \left(\frac{K_{Tc} \times K_T}{\beta_1 K_T + (1 - \beta_1) K_{Tc}} \right) \quad \text{Eq. 34}$$

The overall stiffness of the wall given by $K = K_{P1} + K_{P2}$ Eq. 35

4.2.2 Damage patterns observed on the Flanges of the wall due to bi-directional loading

As we know from the earlier case the wall is subjected to X direction loading first, hence we observe Type 3 damage patterns on the flanges, and once the wall is displaced to the maximum point in X direction, it is then loaded in the Y direction, hence we start observing Type 1 or Type 2 (based on the position of the wall) damages over the already existing damages on the flanges. (As shown in the figures 41)

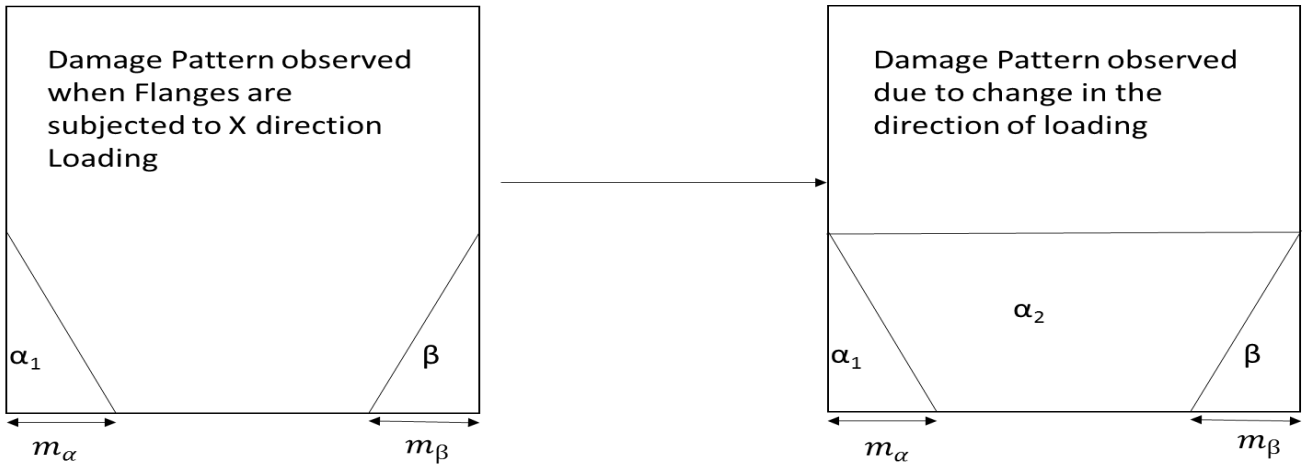

Figure 41: Damage pattern observed in flanges due to change in direction of loading

The position of $h_{\alpha 2}$ (i.e. height of the secondary damage zone of α_2) can vary in three ways as shown in figure 42

4.2.2(a): α_1 triangle forming on the left and β damage triangle on the right

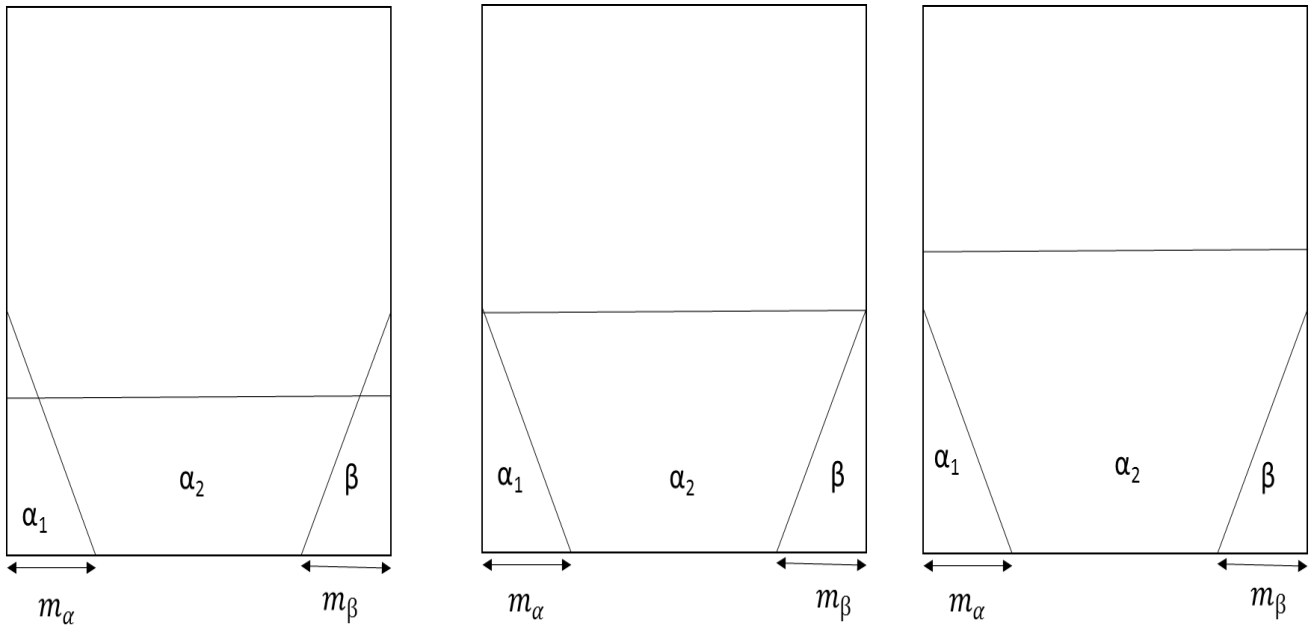

Figure 42: All possible damage cases in flanges observed

Case 1: $h_{\alpha 1} > h_{\alpha 2}$ *and* $h_{\alpha 2} < h_{\beta 1}$

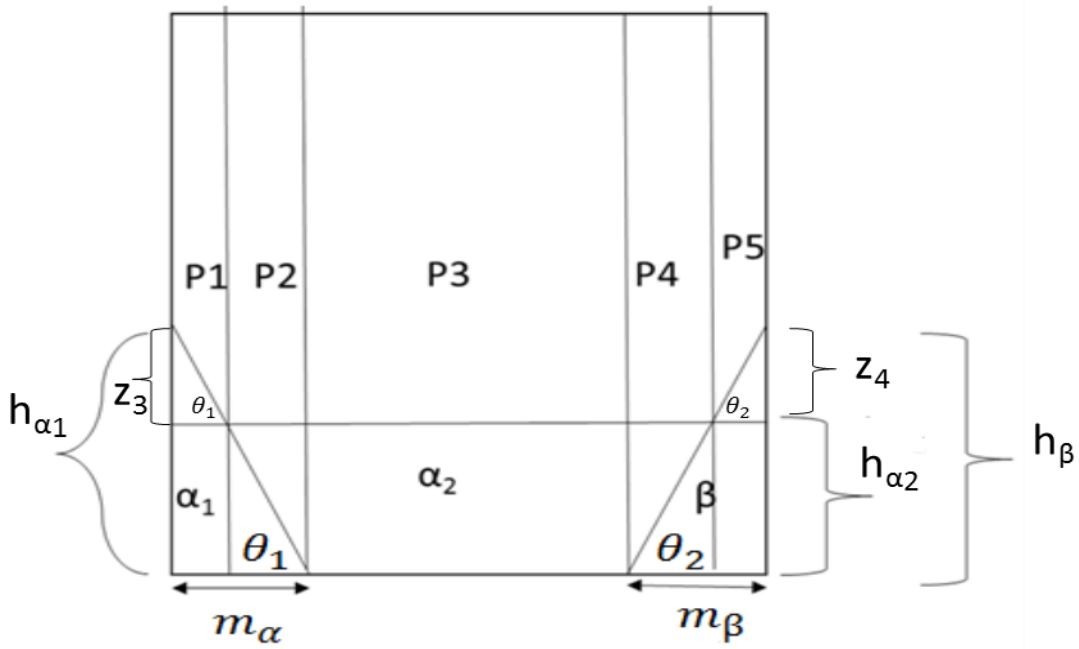

Figure 43: Case 1 $h_{\alpha 1} > h_{\alpha 2}$ *and* $h_{\alpha 2} < h_{\beta 1}$

The wall surface can be divided into five parts, and the overall stiffness is addition of the stiffness due to all the parts.

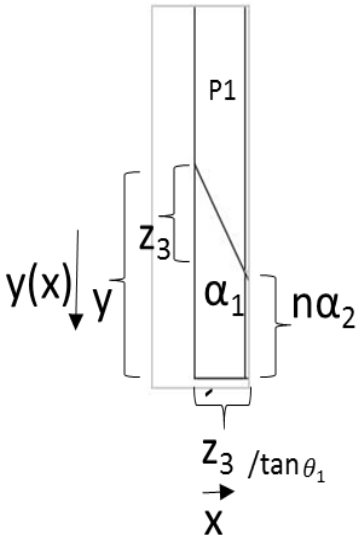

Figure 43(a) Part 1

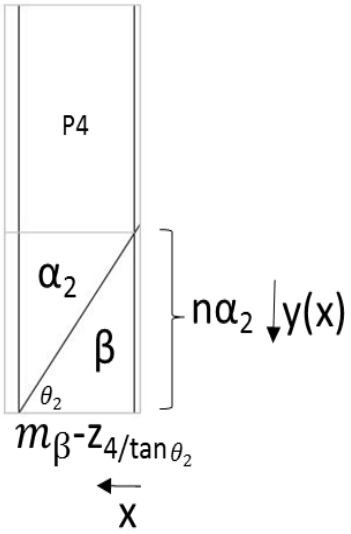

Figure 43(b): Part 4

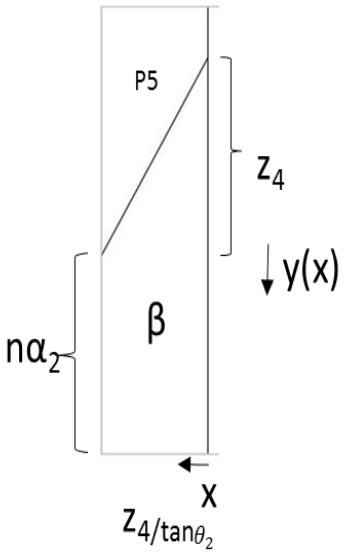

Figure 43(c): Part 5

Part 1:

$$K_{P1} = \sum_{x=0}^{x=z_3/tan\theta_1} \frac{K_T \times K_{Ty}}{[n - y(x)]K_{Ty} + y(x)K_T} \qquad \text{Eq. 36}$$

where $z_3 = (\frac{2\times\alpha_1\times m\times n}{m_\alpha}) - (n\times\alpha_2)$ and $y(x) = (\frac{2\times\alpha_1\times m\times n}{m_\alpha}) - x tan\theta_1$

Here $tan\theta_1 = \frac{2\times\alpha_1\times m\times n}{m_\alpha^2} = \frac{h_{\alpha_1}}{m_\alpha}$

Part2:

$$K_{P2} = \frac{m_\alpha - z_3/tan\theta_1}{n} \times \left(\frac{K_{Ty}\times K_T}{\alpha_2 K_T + (1 - \alpha_2)K_{Ty}}\right) \qquad \text{Eq. 37}$$

Part3:

$$K_{P3} = \frac{m - m_\alpha - m_\beta}{n} \times \left(\frac{K_{Ty}\times K_T}{\alpha_2 K_T + (1 - \alpha_2)K_{Ty}}\right) \qquad \text{Eq. 38}$$

Part4:

As you can see from Figures 43 and Figure 43(b), the y value keeps decreasing as we move from right to left. Hence y value in terms of x can be written as follows

$$y(x) = n\times\alpha_2 - x\tan\theta_2$$

where the number of horizontal cells, x ranges from 0 to $m_\beta - z_4/tan\theta_2$. In a vertical row of unit cells, y (x) cells will have a stiffness equal to K_{Tc} and (n×α_2 – y (x)) cells will have a stiffness equal to K_{Ty} and (n- n×α_2) cells have a stiffness equal to K_T. Hence the stiffness for a single series of cells can be determined as

$$\frac{1}{K} = \frac{y(x)}{K_{Tc}} + \frac{n\times\alpha_2 - y(x)}{K_{Ty}} + \frac{n - n\times\alpha_2}{K_T}$$

By simplifying the above equation, we get

$$K_{P4} = \sum_{x=0}^{x= m_\beta - z_4/tan\theta_2} \frac{K_T\times K_{Ty}\times K_{Tc}}{[n\times\alpha_2 - y(x)]K_T K_{Tc} + y(x)K_T K_{Ty} + (n - n\times\alpha_2)K_{Ty}K_{Tc}} \quad \text{Eq. 39}$$

where $z_4 = (\frac{2\times\beta\times m\times n}{m_\beta}) - (n\times\alpha_2)$

For Part5:

$$K_{P5} = \sum_{x=0}^{x=z_4/tan\theta_2} \frac{K_T\times K_{Tc}}{[n - y(x)]K_{Tc} + y(x)K_T} \quad \text{Eq. 40}$$

where $z_4 = (\frac{2\times\beta\times m\times n}{m_\beta}) - (n\times\alpha_2)$ and $y(x) = (\frac{2\times\beta\times m\times n}{m_\beta}) - xtan\theta_2$

Here, $tan\theta_2 = \frac{2\times\beta\times m\times n}{m_\beta^2} = \frac{h_\beta}{m_\beta}$

Therefore, the overall stiffness of the wall surface

$$(K) = K_{P1} + K_{P2} + K_{P3} + K_{P4} + K_{P5} \quad \text{Eq. 41}$$

Case 2: $h_{\alpha 1} = h_{\alpha 2}$ *and* $h_{\alpha 2} = h_{\beta 1}$

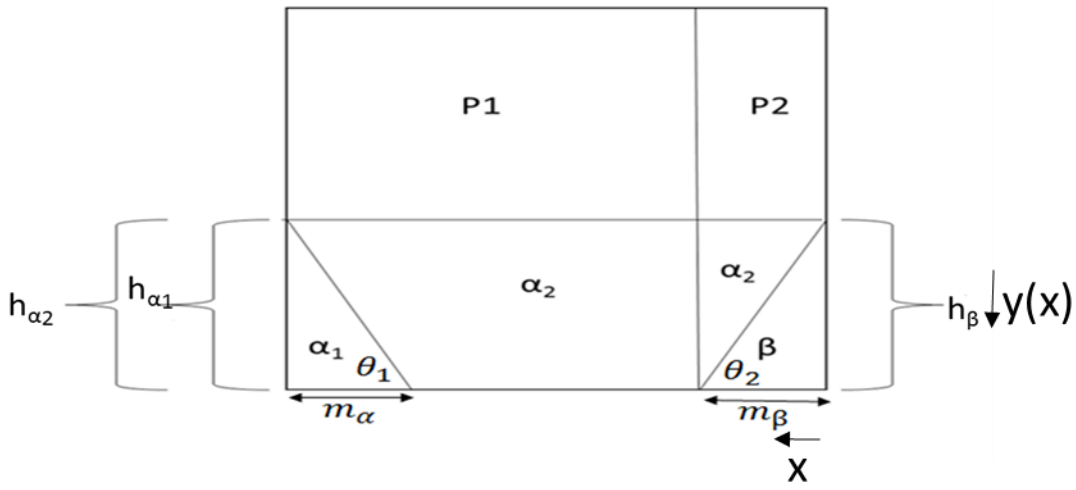

Figure 44: Case 2 when $h_{\alpha 1} = h_{\alpha 2}$ and $h_{\alpha 2} = h_\beta$

For this case we divide the wall surface into 2 parts

Part 1:

$$K_{P1} = \frac{m - m_\beta}{n} \times \left(\frac{K_{Ty} \times K_T}{\alpha_2 K_T + (1 - \alpha_2) K_{Ty}} \right) \qquad \text{Eq. 42}$$

Part 2:

As you can see from Figures 44, the y value keeps decreasing as we move from right to left. Hence y value in terms of x can be written as follows

$$y(x) = n \times \alpha_2 - x \tan\theta_2$$

where the number of horizontal cells, x ranges from 0 to m_β .In a vertical row of unit cells, y (x) cells will have a stiffness equal to K_{Tc} and (n×α_2 – y (x)) cells will have a stiffness equal to K_{Ty} and (n- n×α_2) cells have a stiffness equal to K_T. Hence the stiffness for a single series of cells can be determined as

$$\frac{1}{K} = \frac{y(x)}{K_{Tc}} + \frac{n \times \alpha_2 - y(x)}{K_{Ty}} + \frac{n - n \times \alpha_2}{K_T}$$

By simplifying the above equation, we get

$$K_{P2} = \sum_{x=0}^{x=m_\beta} \frac{K_T \times K_{Ty} \times K_{Tc}}{[n \times \alpha_2 - y(x)]K_T K_{Tc} + y(x) K_T K_{Ty} + (n - n \times \alpha_2) K_{Ty} K_{Tc}} \quad \text{Eq. 43}$$

where $tan\theta_2 = \frac{2 \times \beta \times m \times n}{m_\beta^2}$ and $y(x) = n \times \alpha_2 - x tan\theta_2$

Therefore, the overall stiffness of the wall surface *(K)* = $K_{P1} + K_{P2}$ Eq. 44

Case 3: $h_{\alpha 1} < h_{\alpha 2}$ and $h_{\alpha 2} > h_{\beta 1}$

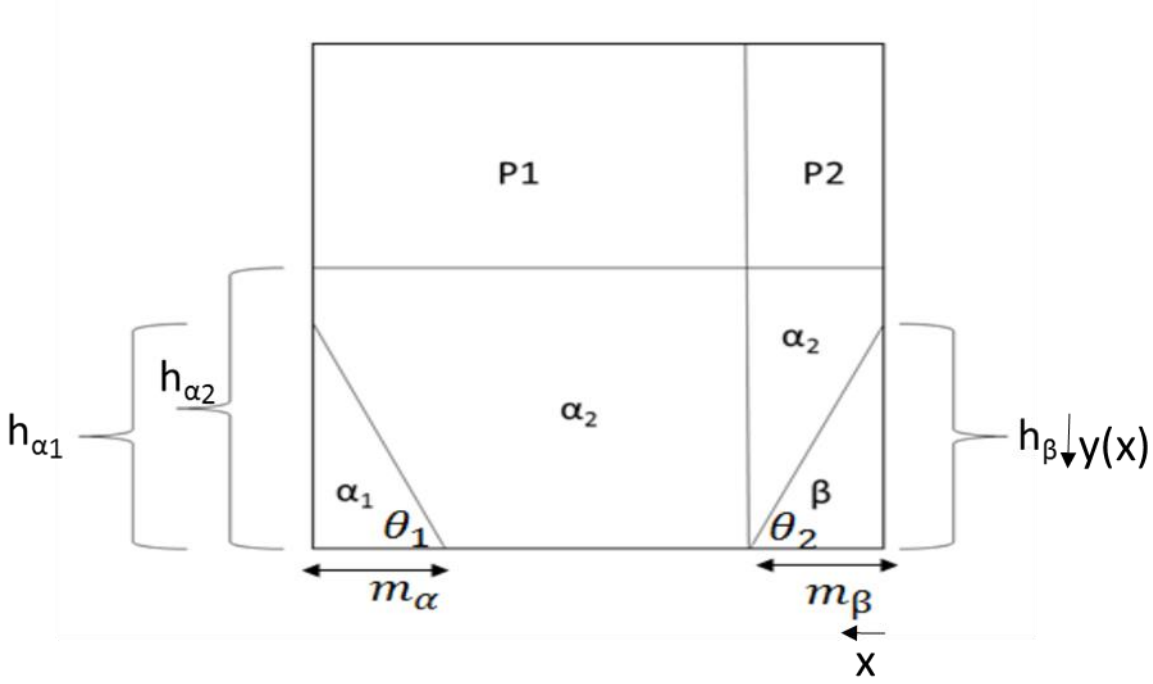

Figure 45: $h_{\alpha 1} < h_{\alpha 2}$ and $h_{\alpha 2} > h_\beta$

For this case, we divide the wall surface into two parts

Part 1:

$$K_{P2} = \frac{m - m_\beta}{n} \times \left(\frac{K_{Ty} \times K_T}{\alpha_2 K_T + (1 - \alpha_2) K_{Ty}} \right) \quad \text{Eq. 45}$$

Part 2:

As you can see from Figures 45, the y value keeps decreasing as we move from right to left. Hence y value in terms of x can be written as follows

$$y(x) = \frac{2\times\beta\times m\times n}{m_\beta} - x\tan\theta_2$$

where the number of horizontal cells, x ranges from 0 to m_β .In a vertical row of unit cells, y (x) cells will have a stiffness equal to K_{Tc} and (n×α_2 – y (x)) cells will have a stiffness equal to K_{Ty} and (n- n×α_2) cells have a stiffness equal to K_T. Hence the stiffness for a single series of cells can be determined as

$$\frac{1}{K} = \frac{y(x)}{K_{Tc}} + \frac{n\times\alpha_2 - y(x)}{K_{Ty}} + \frac{n - n\times\alpha_2}{K_T}$$

By simplifying the above equation, we get

$$K_{P3} = \sum_{x=0}^{x=m_\beta} \frac{K_T\times K_{Ty}\times K_{Tc}}{[n\times\alpha_2 - y(x)]K_T K_{Tc} + y(x)K_T K_{Ty} + (n - n\times\alpha_2)K_{Ty}K_{Tc}} \quad \text{Eq. 46}$$

$$tan\theta_2 = \frac{2\times\beta\times m\times n}{m_\beta^2} = \frac{h_\beta}{m_\beta}$$

Therefore, the overall stiffness of the wall surface *(K)* = K_{P1} + K_{P2} Eq. 47

4.2.2(b): α_1 triangle forming on the right and β damage triangle on the left

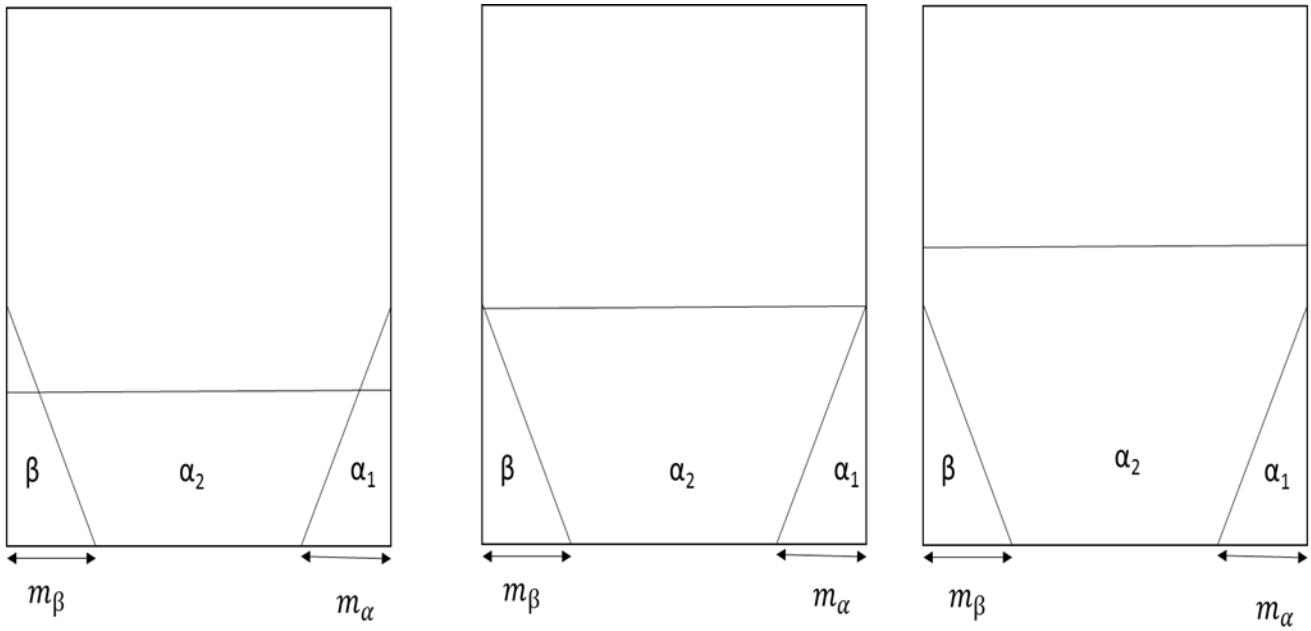

Figure 46: Possible damage cases in flanges observed

Case 1: $h_{\alpha 1} > h_{\alpha 2}$ *and* $h_{\alpha 2} < h_{\beta 1}$

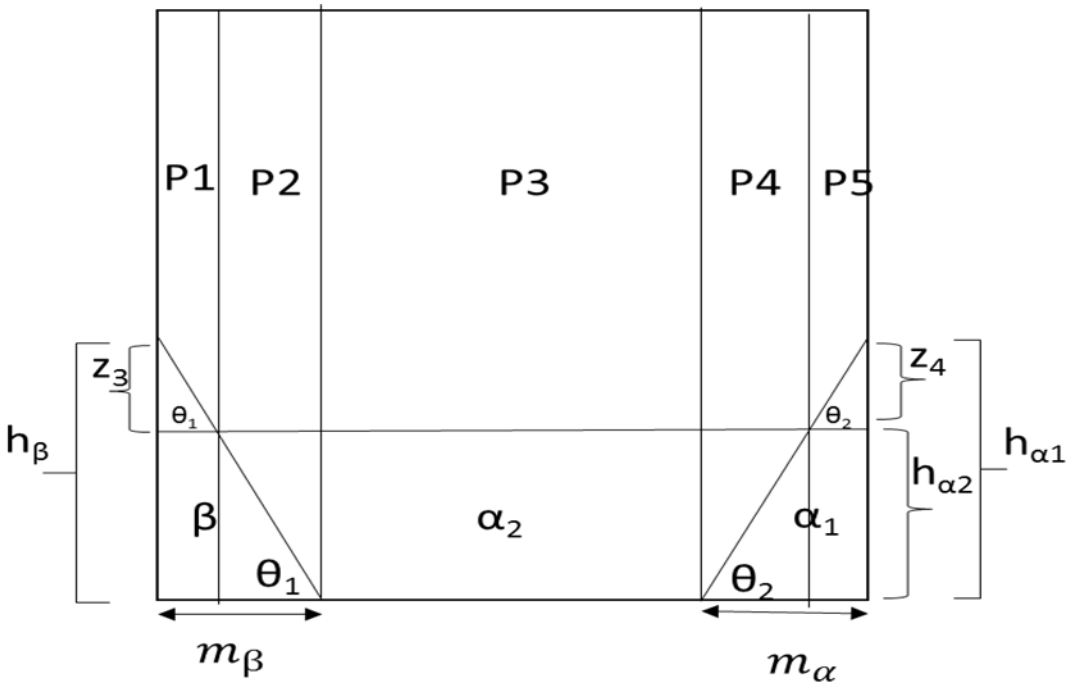

Figure 47: Case 1: $h_{\alpha 1} > h_{\alpha 2}$ and $h_{\alpha 2} < h_{\beta 1}$

The wall surface can be divided into five parts, and the overall stiffness is addition of the stiffness due to all parts.

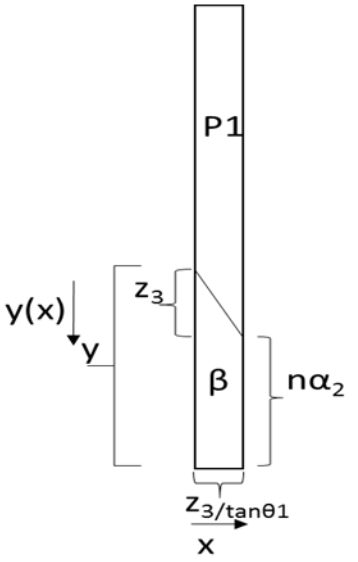

Figure 47(a) Part 1

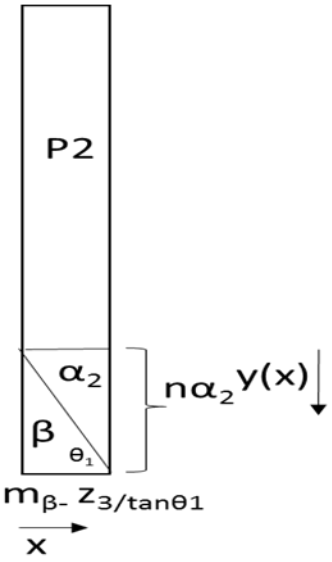

Figure 47(b) Part 2

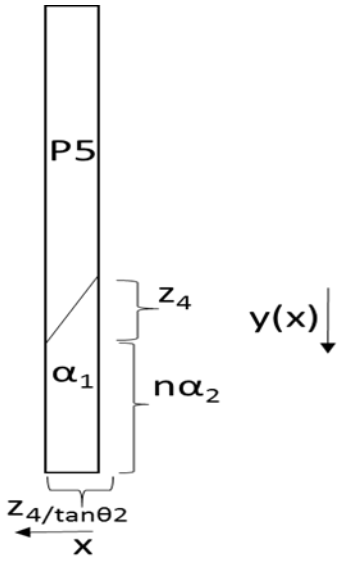

Figure 47(c) Part 5

Part 1:

$$K_{P1} = \sum_{x=0}^{x=z_3/tan\theta_1} \frac{K_T \times K_{Tc}}{[n - y(x)]K_{Tc} + y(x)K_T} \quad \text{Eq. 48}$$

Where $z_3 = (\frac{2\times\beta\times m\times n}{m_\beta}) - (n\times\alpha_2)$ and $y(x) = (\frac{2\times\beta\times m\times n}{m_\beta}) - x tan\theta_1$

Here, $tan\theta_1 = \frac{2\times\beta\times m\times n}{m_\beta^2} = \frac{h_\beta}{m_\beta}$

Part 2:

As you can see from Figures 47 and Figure 47(b), the y value keeps decreasing as we move from left to right. Hence y value in terms of x can be written as follows

$$y(x) = n\times\alpha_2 - x\tan\theta_1$$

where the number of horizontal cells, x ranges from 0 to $m_\beta - z_3/tan\theta_1$. In a vertical row of unit cells, y (x) cells will have a stiffness equal to K_{Tc} and (n×α_2 – y (x)) cells will have a stiffness equal to K_{Ty} and (n- n×α_2) cells have a stiffness equal to K_T. Hence the stiffness for a single series of cells can be determined as

$$\frac{1}{K} = \frac{y(x)}{K_{Tc}} + \frac{n\times\alpha_2 - y(x)}{K_{Ty}} + \frac{n - n\times\alpha_2}{K_T}$$

By simplifying the above equation, we get

$$K_{P2} = \sum_{x=0}^{x= m_\beta - z_3/tan\theta_1} \frac{K_T \times K_{Ty} \times K_{Tc}}{[n\times\alpha_2 - y(x)]K_T K_{Tc} + y(x)K_T K_{Ty} + (n - n\times\alpha_2)K_{Ty}K_{Tc}} \quad \text{Eq. 49}$$

Where $z_3 = (\frac{2\times\beta\times m\times n}{m_\beta}) - (n\times\alpha_2)$

Part 3:

$$K_{P3} = \frac{m - m_\alpha - m_\beta}{n} \times \left(\frac{K_{Ty}\times K_T}{\alpha_2 K_T + (1 - \alpha_2)K_{Ty}}\right) \quad \text{Eq. 50}$$

Part 4:

$$K_{P4} = \frac{m_\alpha - z_4/tan\theta_2}{n} \times \left(\frac{K_{Ty} \times K_T}{\alpha_2 K_T + (1 - \alpha_2) K_{Ty}} \right) \quad \text{Eq. 51}$$

Where $z_4 = (\frac{2 \times \alpha_1 \times m \times n}{m_\alpha}) - (n \times \alpha_2)$ and $tan\theta_2 = \frac{2 \times \alpha_1 \times m \times n}{m_\alpha^2} = \frac{h_{\alpha_1}}{m_\alpha}$

Part 5:

$$K_{P5} = \sum_{x=0}^{x=z_4/tan\theta_2} \frac{K_T \times K_{Ty}}{[n - y(x)]K_{Ty} + y(x)K_T} \quad \text{Eq. 52}$$

Where $z_4 = (\frac{2 \times \alpha_1 \times m \times n}{m_\alpha}) - (n \times \alpha_2)$ and $y(x) = (\frac{2 \times \alpha_1 \times m \times n}{m_\alpha}) - x tan\theta_2$

Here $tan\theta_2 = \frac{2 \times \alpha_1 \times m \times n}{m_\alpha^2} = \frac{h_{\alpha_1}}{m_\alpha}$

Therefore, the overall stiffness of the wall surface

$$(K) = K_{P1} + K_{P2} + K_{P3} + K_{P4} + K_{P5} \quad \text{Eq. 53}$$

Case 2: $h_{\alpha 1} = h_{\alpha 2}$ *and* $h_{\alpha 2} = h_{\beta 1}$

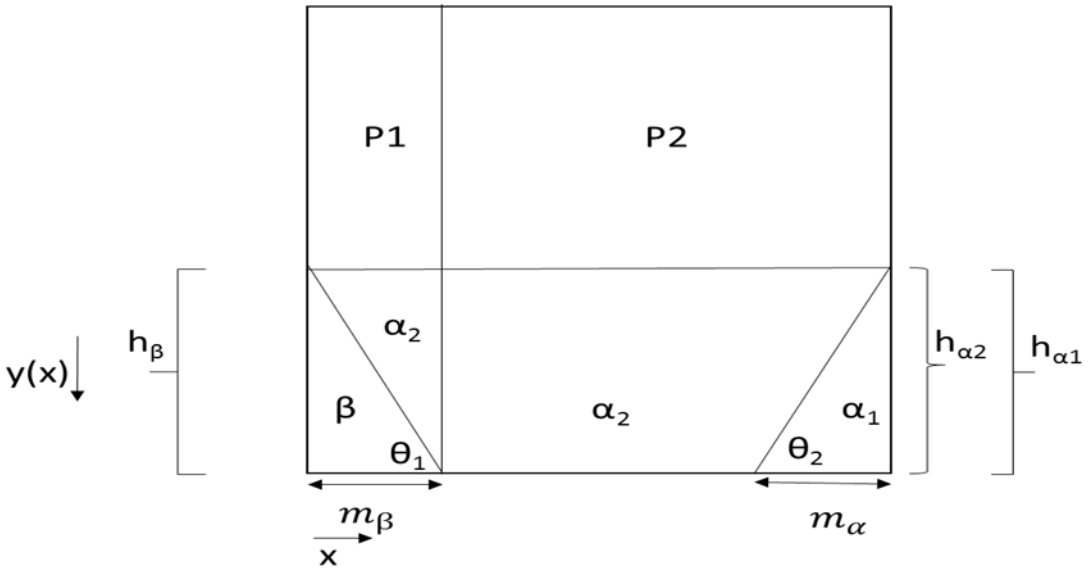

Figure 48: Case 2 when $h_{\alpha 1} = h_{\alpha 2}$ and $h_{\alpha 2} = h_\beta$

Part 1:

As you can see from Figures 48, the y value keeps decreasing as we move from left to right. Hence y value in terms of x can be written as follows

$$y(x) = n \times \alpha_2 - x\tan\theta_1$$

where the number of horizontal cells, x ranges from 0 to m_β. In a vertical row of unit cells, y (x) cells will have a stiffness equal to K_{Tc} and (n×α_2 – y (x)) cells will have a stiffness equal to K_{Ty} and (n- n×α_2) cells have a stiffness equal to K_T. Hence the stiffness for a single series of cells can be determined as

$$\frac{1}{K} = \frac{y(x)}{K_{Tc}} + \frac{n \times \alpha_2 - y(x)}{K_{Ty}} + \frac{n - n \times \alpha_2}{K_T}$$

By simplifying the above equation, we get

$$K_{P1} = \sum_{x=0}^{x=m_\beta} \frac{K_T \times K_{Ty} \times K_{Tc}}{[n \times \alpha_2 - y(x)]K_T K_{Tc} + y(x)K_T K_{Ty} + (n - n \times \alpha_2)K_{Ty} K_{Tc}} \quad \text{Eq. 54}$$

Where $tan\theta_1 = \frac{2 \times \beta \times m \times n}{m_\beta^2} = \frac{h_\beta}{m_\beta}$ and $y(x) = n \times \alpha_2 - x\tan\theta_1$

Part 2:

$$K_{P1} = \frac{m - m_\beta}{n} \times \left(\frac{K_{Ty} \times K_T}{\alpha_2 K_T + (1 - \alpha_2)K_{Ty}} \right) \quad \text{Eq. 55}$$

Therefore, the overall stiffness of the wall surface

$$(K) = K_{P1} + K_{P2} \quad \text{Eq. 56}$$

Case 3: $h_{\alpha 1} < h_{\alpha 2}$ and $h_{\alpha 2} > h_{\beta 1}$

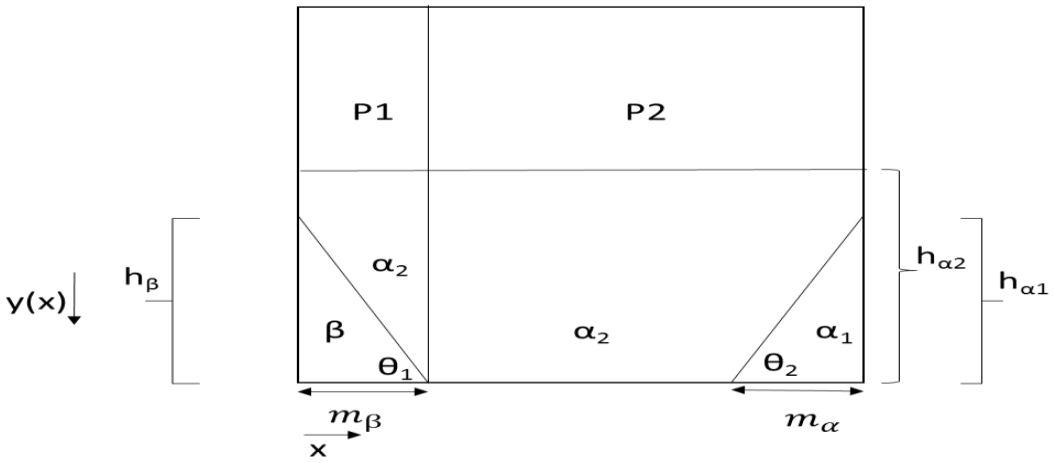

Figure 49: $h_{\alpha 1} < h_{\alpha 2}$ and $h_{\alpha 2} > h_\beta$

Part 1:

As you can see from Figures 49, the y value keeps decreasing as we move from left to right. Hence y value in terms of x can be written as follows

$$y(x) = n\times\alpha_2 - x\tan\theta_1$$

where the number of horizontal cells, x ranges from 0 to m_β. In a vertical row of unit cells, y (x) cells will have a stiffness equal to K_{Tc} and (n×α2 – y (x)) cells will have a stiffness equal to K_{Ty} and (n- n×α2) cells have a stiffness equal to K_T. Hence the stiffness for a single series of cells can be determined as

$$\frac{1}{K} = \frac{y(x)}{K_{Tc}} + \frac{n\times\alpha_2 - y(x)}{K_{Ty}} + \frac{n - n\times\alpha_2}{K_T}$$

By simplifying the above equation, we get

$$K_{P1} = \sum_{x=0}^{x=m_\beta} \frac{K_T\times K_{Ty}\times K_{Tc}}{[n\times\alpha_2 - y(x)]K_T K_{Tc} + y(x)K_T K_{Ty} + (n - n\times\alpha_2)K_{Ty}K_{Tc}} \quad \text{Eq. 57}$$

Where $tan\theta_1 = \frac{2\times\beta\times m\times n}{m_\beta^2} = \frac{h_\beta}{m_\beta}$ and $y(x) = n\times\alpha_2 - x\tan\theta_1$

Part 2:

$$K_{P1} = \frac{m - m_\beta}{n}\times\left(\frac{K_{Ty}\times K_T}{\alpha_2 K_T + (1 - \alpha_2)K_{Ty}}\right) \quad \text{Eq. 58}$$

Therefore, the overall stiffness of the wall surface

$$(K) = K_{P1} + K_{P2} \quad \text{Eq. 59}$$

CHAPTER 5

VALIDATION AND PARAMETRIC STUDY

5.1 Validation of the spring molecule for unidirectional loading.

The overall stiffness of the wall is assumed to be the addition of stiffness of each wall surface (i.e., one Web and 2 Flanges) at that particular drift obtained from the equations derived from Chapter 4.

$$K_{Wall} = K_{web} + K_{Flange} + K_{Flange}$$

$$K_{O\_Wall} = K_{O\_web} + K_{O\_Flange} + K_{O\_Flange}$$

Note: In reality, we do not have steel in each and every cell of the spring cell molecule. Hence, the *Ks* of the steel has been reduced by multiplying it by the vertical steel reinforcement ratio (ρ) which is equal to 0.0056 [13]. The yield strength of rebars, compressive strength of concrete and other material properties were obtained from Ile [13].

5.1.1 **Determining the K_{Wall} with increasing drift ratios for Wall1(i.e. Y-direction loading)**

XZ Plane: we observe Type 1 and Type 2 damages on XZ plane of Wall1 based on position of wall under Y direction loading. The observed α and β values with increasing drift ratio's is shown in Figure 19. Using these values in equations 4 and 6 respectively, K_{XZ} (stiffness of XZ plane) with increasing drift ratios under tension and compression can be computed.

YZ Plane: We observe Type 3 damage on YZ plane of Wall1. The observed α, β, m_α and m_β values is shown in figures 20(a),20(b), 21 and 22. Using these values in equations 7, 8, 9, 10 and 11. K_{YZ} (stiffness of YZ plane) with increasing drift ratios under tension and compression can be computed. The K_{Wall} is equal to K_{XZ} + K_{XZ} + K_{YZ} at each drift ratio point.

The initial stiffness for each surface (XZ and YZ plane) is determined Eq.2. The total initial stiffness is equal to $K_{O\_Wall} = K_{O\_YZ} + K_{O\_XZ} + K_{O\_XZ}$

Ratio between K_{Wall} and K_{O_Wall} of Wall1 is obtained with increasing drift ratio and a graph is ploted as shown in Figure 50. Comparision has been made between the experimental stiffness reduction ratio and computed value for Wall 1 as seen in figure 50. The experimental stiffness reduction ratio was determined using the force displacement graph obtained from VEEL. By

determing the slope between two consecutive peeak displacements in the FD curve we get the stiffness value and when it is divided with the initial stiffness we get stiffness reduction factor experimentally.

5.1.2 **Determing the K_{Wall} with increasing drift ratios for Wall2 (i.e. X-direction loading)**

YZ Plane: We onserve Type 1 and Type 2 damages on YZ plane of Wall2 based on the position of wall during X direction loading and the observed α and β values with increasing drift ratio's is shown in Figure 25. Using these values in equations 4 and 6 respectively, K_{YZ} (stiffness of YZ plane) with increasing drift ratios under tension and compression can be computed.

XZ Plane: We observe Type 3 damage on this surface. The observed α, β, m_α and m_β values is shown in figures 23(a),23(b), and 24. Using these values in equations 7, 8, 9, 10 and 11. K_{XZ} (stiffness of XZ plane) with increasing drift ratios under tension and compression can be computed. The K_{Wall} is equal to K_{XZ} + K_{XZ} + K_{YZ} at each drift ratio point

Similar to Wall1, The initial stiffness for each surface (XZ and YZ plane) is determined Eq.2. The total initial stiffness is equal to $K_{O\_Wall} = K_{O\_YZ} + K_{O\_XZ} + K_{O\_XZ}$

Ratio between K_{Wall} and K_{O_Wall} of Wall2 is obtained with increasing drift ratio and a graph is ploted as shown in Figure 51. Comparision has been made between the experimental stiffness reduction ratio and computed value for Wall 2 as seen in figure 51.

Looking into the two graphs, we can conclude that the spring molecule forrmulae is a reasonable model for computing the stiffness reduction factor for non-rectangular shear walls under Uni- and Bi-directional loading.

Wall 1

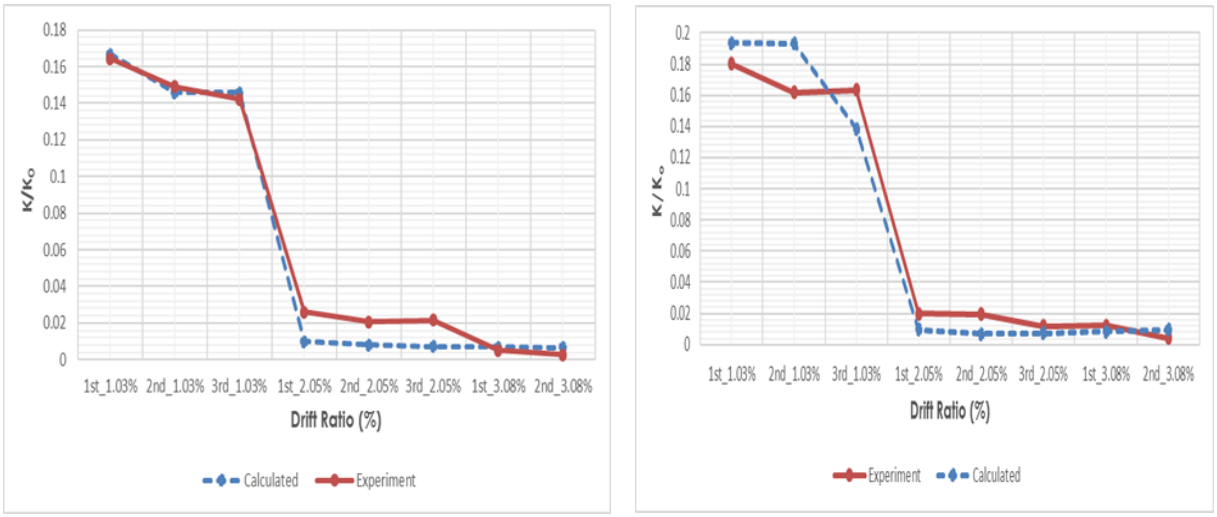

Figure 50: Comparing the experimental and computed stiffness reduction ratio for Wall1 under tension (Left) and compression (Right)

f) Wall 2

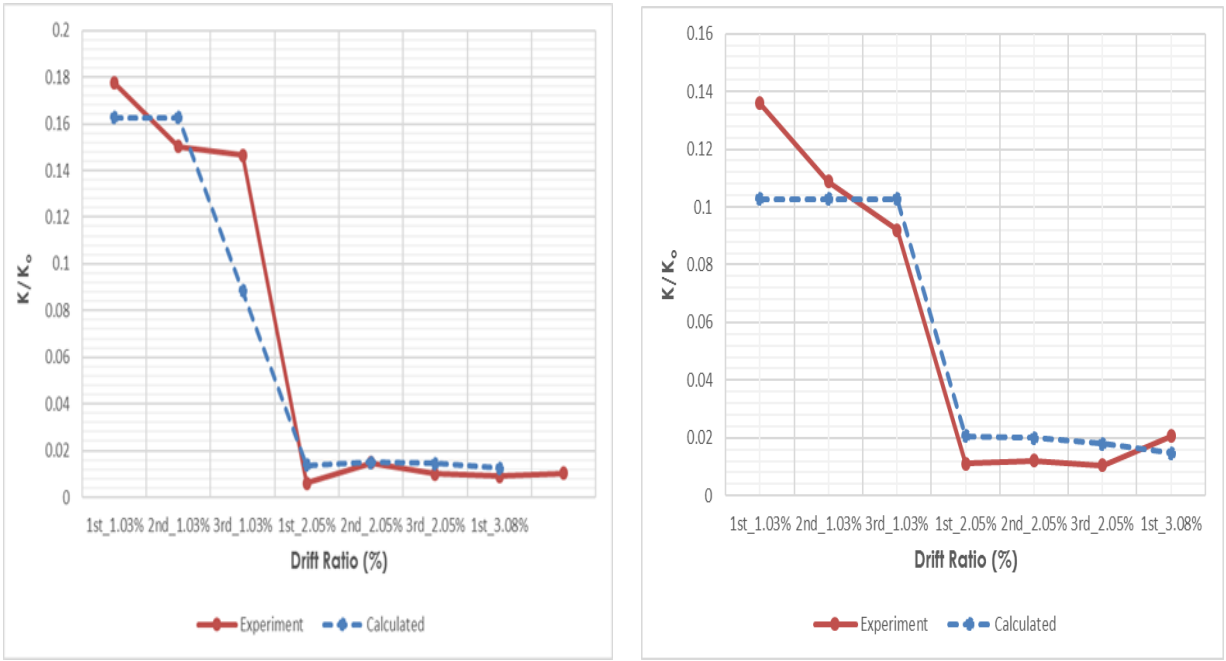

Figure 51: Comparing the experimental and computed stiffness reduction for Wall2 under tension (Left) and compression (Right)

From the two comparisons, we see that there is a slight deviation between the experimental and computed stiffness reduction ratio for Wall 2 (X- direction loading) under tension as well as compression. This deviation may be associated with the unsymmetrical loading direction of the

wall which the spring molecule cannot capture. This spring model is based on several assumptions; hence it needs to be developed further more to capture the stiffness reduction exactly.

5.2 Parametric Study:

To determine the Optimal Setting

A U-shaped wall under biaxial loading, predicts lower capacity in both the directions (X and Y direction) compared to its ability under one direction as shown in figure 9(a) and 9(b). In our case, the U-shaped wall has been subjected to a butterfly pattern loading as illustrated in figure 7 and 8. For simplicity, we will be focusing our discussion only on the first nine steps of the loading pattern i.e. The U-shaped Wall is first loaded in the X direction up to a displacement value of -4cm, now from that position the wall is then subjected to a Y-direction loading up to a displacement of 4cm. Using the observed α, β values under Uni-direction loading and the equations derived from above chapter 4.2. We tried to predict the secondary stiffness of the Wall and compare it to the experimental result obtained from VEEL simulation.

To exactly predict the experimental secondary stiffness. A parametric study has been performed by varying the cell size ranging from 0.1mm to 10mm and the concrete stiffness reduction factor ranging from -0.000109 to -0.109322, which have been discussed in detail below

5.2.1 Cell Size Parametric Study:

To determine the optimal setting for determining the secondary stiffness. The cell size has been varied as 0.1mm, 0.25mm, 0.5mm, 1mm, 5mm and 10mm. The secondary stiffness obtained for each of the cases is shown in Table 4 and Figure 52. The comparison graphs have been divided into two categories because as we can see from the table, the stiffness value varies from x 10^6 to x 10^9. Due to this high range of values, it is quite difficult to plot it on a single graph. Cell sizes from 0.1mm to 0.5mm were plotted in one graph and the other cases 1mm, 5mm, and 10mm are plotted in other cases.

Table 4: Cell Size Parametric Study Displacement (m)

Cell Size (mm)	0.01	0.02	0.03	0.04
0.1	2.17E+07	1.20E+07	8.59E+06	6.14E+06
0.25	2.79E+07	1.63E+07	1.24E+07	9.58E+06
0.5	4.00E+07	2.07E+07	1.52E+07	1.18E+07
1	5.45E+08	3.40E+08	2.08E+08	1.37E+07
5	4.04E+09	2.85E+09	1.97E+08	1.65E+08
10	9.32E+09	7.77E+09	6.85E+09	5.98E+09

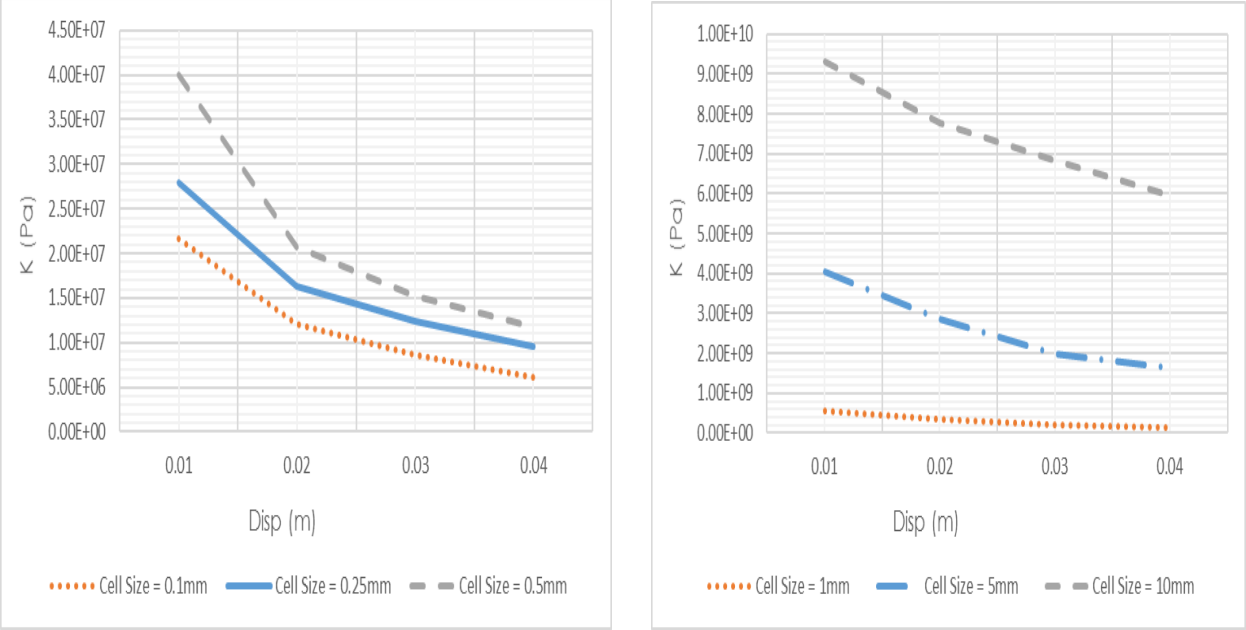

Figure 52: Cell Size Parametric Study Comparison

From Figure 52, we can conclude that the model is mesh sensitive and as the cell size increases the secondary stiffness value increases. We can also conclude that the cell size should be less than 1 for better results as can be seen from the two graphs above, when the cell size increases from 0.1 to 0.5mm there is only slight increase in the secondary stiffness, but when we increase it from 1mm to 10mm the stiffness increase is enormous.

5.2.2 Concrete stiffness reduction factor (d) parametric study

The concrete stiffness reduction factor (d) determined using the Kent and Park Model as shown in chapter 3, is equal to -0.109322, to find the optimal setting for determining secondary stiffness, the d value changed from -0.000109322 to -0.109322. The results obtained are summarized in Table 5 and Figure 53.

Table 5: Concrete Stiffness reduction factor parametric study

d value	0.01	0.02	0.03	0.04
-1.09322E-04	1.52E+07	9.44E+06	7.94E+06	5.53E+06
-1.09322E-03	2.79E+07	1.63E+07	1.24E+07	9.58E+06
-1.09322E-02	1.51E+08	9.37E+07	6.69E+07	5.06E+07
-1.03922E-01	1.28E+09	8.38E+08	3.64E+08	1.55E+08

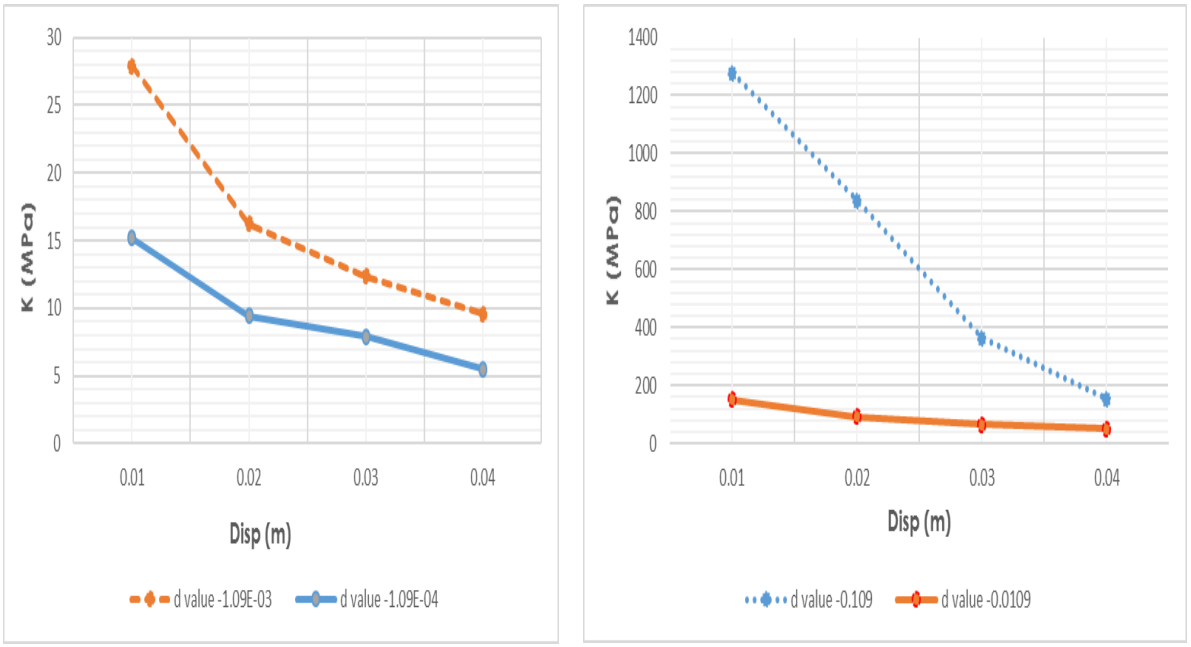

Figure 53: Concrete Stiffness Reduction factor (d) – parametric study

From the two parametric studies, the optimal setting for this particular case is a d value equal to -0.00109322 and a cell size equal to 0.25mm

5.3 Validation for Uni-directional loading

Using the optimal setting determined earlier, validation for stiffness reduction in one-directional loading was done, and the results are shown in figure 54 and 55

5.3.1 Wall 1:

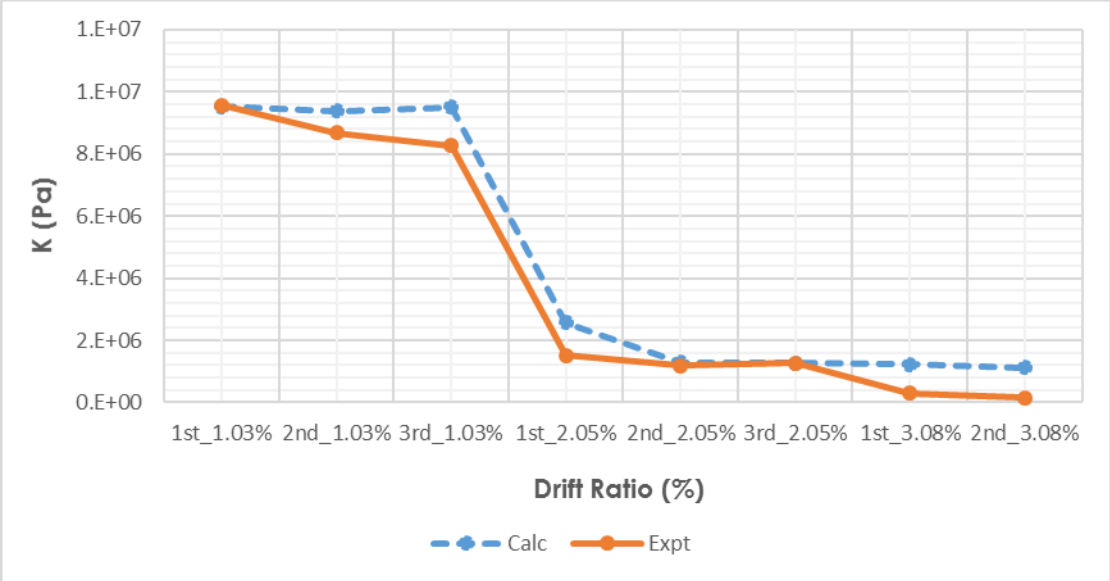

Figure 54: Comparison of Wall1 Stiffness reduction using the optimal setting

5.3.2 Wall2:

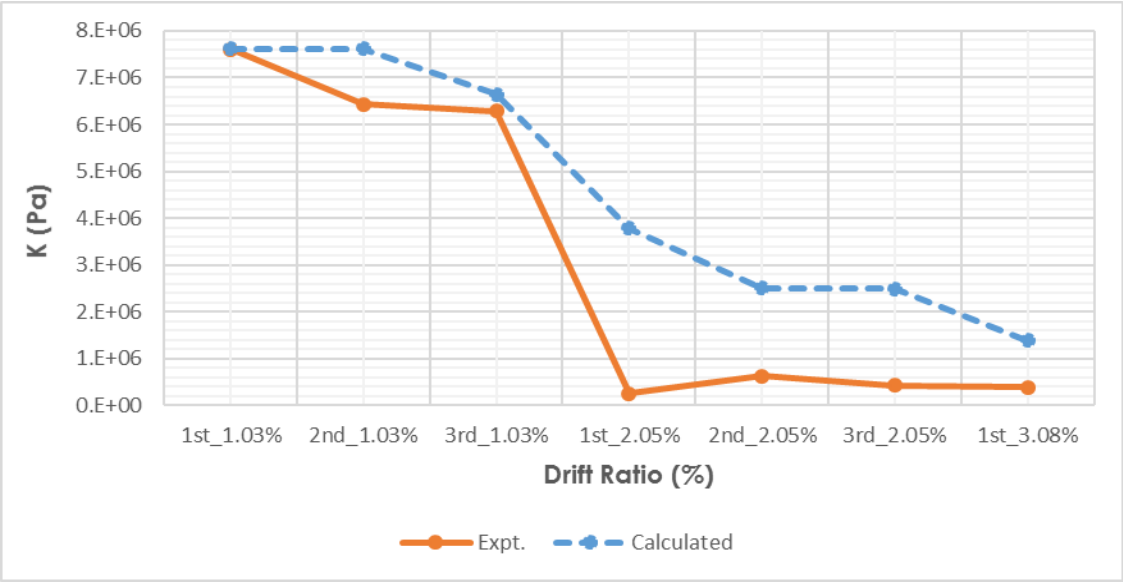

Figure 55: Comparison of Wall2 Stiffness reduction using optimal setting

From the Figures 54 and 55, we can conclude the optimal setting determined for bi-axial loading, satisfies very well with one directional loading. The overall shape and value for Wall1 under tension coincides very well with the experimental result, whereas in Case2 the results deviated from each other, one plausible reason for this deviation is that the Wall2 is loaded in X direction which is unsymmetrical loading. The spring model is not able to consider the unsymmetrical loading. Hence further research is required on the spring model to develop a realistic approach to tackling the overlapping damage states so as to predict the realistic behavior of non-rectangular shear walls. From the satisfactory unidirectional loading results, an attempt is made to extend the spring molecule model to bidirectional loading using the same optimal setting used for unidirectional loading which is discussed in the next chapter.

CONCLUSION

In an attempt to find a unified stiffness (damage) reduction factor for U-shaped walls under bi-directional loading, this study developed equations based on different damage states that are plausible on the web and flanges of the U-shaped wall. A novel technique of spring molecule model has been developed which divides the rectangular surface into m by n cells aligned vertically. Each cell consisting of a nonlinear spring and a nonlinear compressive concrete spring with a compression-only gap. The results show that the equations are reasonably good to monitor the secondary stiffness of U-shaped walls under biaxial loading. Parametric study on the cell size and concrete stiffness reduction factor has been done to determine the optimal setting. The spring model seems to be a good starting point to consider secondary stiffness reductions for other non-rectangle shape walls like L- and T-shaped walls. The equations coincide well with experimental results under uniaxial loads. Also, an application to a U-shaped wall under bi-directional loading showed a promising possibility of the developed method.

FUTURE RESEARCH

This spring molecule model assumption promises to be a reasonable starting point to determine stiffness reduction factor quickly for other complex shape walls like the T-, L-, or Box shaped walls. Results call for further validations and sophistications against various experimental researches on complex wall subjected to multi-directional irregular loading conditions.

REFERENCES

1. Alessandro Dazio, Katrin Beyer and Hugo Bachmann. “Quasi-static cyclic tests and plastic hinge analysis of RC structural walls,” *Engineering Structures*. 31, pp.1556-1571; 2009.

2. K. Beyer, A. Dazio, M.J.N Priestley. “Quasi-Static Cyclic Tests of Two U-Shaped Reinforced Concrete Walls,” *Journal of Earthquake Engineering.* vol.12, pp. 1023-1053; 2010.

3. Kerem Gulee and Andrew Whittaker, John Hooper. “Damage States and Fragility Curves for Squat Reinforced Concrete Walls,”

4. Fabio Taucer, Enrico Spacone and Filip C. Filippou. “A Fiber Beam-Column Element for Seismic Response Analysis of Reinforced Concrete Structures,” *report to The National Science Foundation and the California Department of Transportation*. UCB/EERC-17, pp. 23-37; 1997.

5. Xiao Lu, Xinzheng Lu, Hong Guan and Lieping Ye. “Collapse simulation of reinforced concrete high-rise building induced by extreme earthquakes,” *Earthquake Engineering Structural Dynamics*. vol. 42, pp. 705-723, 2012.

6. Eduardo N. Dvorkin, Daniel Pantuso, Eduardo A. Repetto. “A formulation of the MITC4 shell element for finite strain elastoplastic analysis,” *Computer Methods in applied mechanics and engineering*. vol. 125, pp. 17-40; 1995.

7. In Ho Cho and Keith A. Porter. “Structure- Independent Parallel Platform for Nonlinear Analyses of General Real-Scale RC Structures under Cyclic Loading,” *Journal of Structural Engineering*. pp. 1-40, 2013.

8. In Ho Cho. “Virtual Earthquake Engineering Laboratory Capturing Nonlinear Shear, Localized Damage and Progressive Buckling of Bar,” *Earthquake Spectra*. vol.29, pp.103-126; 2013.

9. In Ho Cho and Keith A. Porter. “Multilayered grouping parallel algorithm for multiple-level multiscale analyses,” *International Journal for Numerical Methods in Engineering.* vol. 100, pp. 914-932; 2014.

10. In Ho Cho and Keith Porter. “Three Stage Multiscale Nonlinear Dynamic Analysis Platform for Building- Level Loss Estimation,” *Earthquake Spectra;* 2013.

11. In Ho Cho, Sai Yemmaleni, Ikkyun Song and Keith A. Porter. “Comparative Study on Multiscale Nonlinear Dynamic Analysis of RC Shear Wall Buildings,”

12. In Ho Cho and John F. Hall. “General Confinement Model Based on Nonlocal information,” *Journal of Engineering Mechanics.*vol.140. pp.1-17; 2014.

13. N. Ile and J.M. Reynouard. “Behavior of U-Shaped Walls Subjected to Uniaxial and Biaxial Cyclic Lateral Loading,” *Journal of Earthquake Engineering*. vol. 9. pp. 67-94; 2005.

14. Sriram Aaleti, Beth L. Brueggen, Benton Johnson, Catherine E. French, and Sri Sritharan. “Cyclic Response of Reinforced Concrete Walls with different anchorage details: Experimental Investigation,” *Journal of Structural Engineering*. pp. 1181-1191; 2013.

15. Thomas N. Salonikos, Andreas J. Kappos, loannis A. Tegos, and Georgios G. Penelis. “Cyclic Load Behavior of Low- Slenderness Reinforced Concrete Walls: Design Basis and Test Results,” *ACI Structural Journal.* pp.649-660; 1999.

16. Xinzheng Lu, Linlin Xie, Hong Guan, Yuli Huang, Xiao Lu, “A shear wall element for nonlinear seismic analysis of super-tall buildings using OpenSees,” Finite Elements in Analysis and Design. vol. 98, pp. 14-25, 2015.

17. R. Clough and L.Benuska. “Nonlinear Earthquake Behavior of Tall Buildings.” *Journal of Mechanical Engineering,* ASCE 93(EM 3), pp. 129-146. 1967.

18. T. Takeda, M.A. Sozen and N. Nielsen “Reinforced Concrete Response to Stimulated Earthquakes,” *Journal of Structural Engineering,* ASCE, pp. 2557-2573; 1970.

19. F. Brancaleoni, V. Ciampi and R. Di Antonio “Rate-Type Models for Non-Linear Hysteretic Structural Behavior,” *EUROMECH Colloquium,* Palermo, Italy; 1983.

20. H. Banon, J. Biggs and M. Irvine “Seismic Damage in Reinforced Concrete Frames,” *Journal of Structural Engineering,* ASCE, 107(ST9), pp. 1713-1729; 1981.

21. S. Otani “Inelastic Analysis of RC Frame Structures,” *Journal of the Structural Division,* ASCE, 100(ST7).

22. F.C. Filippou and A. Issa “Nonlinear Analysis of Reinforced Concrete Frames under Cyclic Load Reversals,” *EERC Report 88-12,* Earthquake Engineering, Research Center, Burkley.

23. S. Lai, G. Will and S. Otani. “Model for Inelastic Biaxial Bending of Concrete Members,” *Journal of Structural Engineering,* ASCE, 110(ST11), pp. 2563-2584; 1984.

24. C. Meyer, M.S. Roufaiel and S.G. Arzoumanidis. “Analysis of Damaged Concrete Frames for Cyclic Loads,” *Earthquake Engineering and Structural Dynamics,* vol. 11, pp. 207-228; 1983.

25. M.S.L Roufaiel and C. Meyer. “Analytical Modeling of Hysteretic Behavior of R/C Frames,” *Journal of Structural Engineering,* ASCE, 113(ST3), pp. 429-444; 1987.

26. L.P. Darvall and P. Mendis. “Elastic-Plastic-Softening Analysis of Plane Frames,” *Journal of Structural Engineering,* ASCE, 11(ST4), pp. 871-888; 1985.

27. T. Takayanagi and W. Schnobrich “Non-Linear Analysis of Coupled Wall Systems,” *Earthquake Engineering and Structural Dynamics,* vol.7, pp. 1-22; 1979.

28. M. Mahasuverachai. “Inelastic Analysis of Piping and Tubular Structures,” *EERC Report 82,* Earthquake Engineering Research Center, University of California, Berkley; 1982.

29. F. Legeron, P. Paultre and J. Mazars. “Damage mechanics modeling of the nonlinear seismic behavior of concrete structures,” *Journal of Structural Engineering,* vol. 131; pp. 946-954; 2005.

30. A. Esmaeily and Y Xiao. “Behavior of Reinforced Concrete Columns under variable Axial loads: Analysis,” *ACI Structural Journal,* vol. 102, pp. 736-744; 2005.

31. loannis D. Lefas, Michael D. Kotsovos and Nicholas N. Ambraseys “Behavior of reinforced concrete structural walls: Strength deformation characteristics, and failure mechanism” *ACI Structural Journal,* vol. 87, pp. 23-31; 1990.lls

32. Shyh-Jiann Hwang, W.H. Fang, H.J. Lee and H.W. Yu. “Analytical model for predicting Shear Strength of Squat Walls,” Journal *of Structural Engineering,* vol.127, pp. 43-50, 2001.

33. “Condo Cluster Compute Node Biology Information Technology,." *Iowa State University:* http://www.biology-it.iastate.edu/condo-cluster-compute-nodes